

Exhumation of the Western Cordillera, Ecuador driven by late Miocene subduction of the Carnegie Ridge

Audrey Margirier¹, Manfred R. Strecker², Peter W Reiners³, Stuart N Thomson³, Ismael Casado², Sarah W.M. George³, and Alexandra Patricia Alvarado⁴

¹IDYST

²University of Potsdam

³University of Arizona

⁴IG-EPN

November 24, 2022

Abstract

Cenozoic growth of the Andes has been strongly influenced by subduction dynamics, reactivation of inherited crustal heterogeneities, and the superposed effects of climate. Subduction of the submarine Carnegie Ridge has fundamentally impacted late Cenozoic magmatism and tectonic activity in the northern Andes. Time-temperature inverse modeling of new thermochronological data from the Western Cordillera of Ecuador reveals two phases of cooling separated by isothermal conditions. The first cooling phase immediately postdates early and middle Miocene magmatism in the Western Cordillera and is attributed to post-magmatic thermal relaxation. The second cooling phase started after 6 Ma, which we infer to record the exhumation in the Western Cordillera, coeval with the last cooling phase in the Eastern Cordillera. Based on these findings we posit that the onset of subduction of the Carnegie Ridge at ~6-5 Ma increased plate coupling at the subduction interface and promoted shortening and regional rock uplift in the northern Andes. Overall, our results highlight the essential role of bathymetric anomalies in driving regional upper-plate deformation at non-collisional convergent plate margins.

Exhumation of the Western Cordillera, Ecuador, driven by late Miocene subduction of the Carnegie Ridge

Audrey Margirier ^{1*}, Manfred R. Strecker¹, Peter W. Reiners ², Stuart N. Thomson ², Ismael Casado ¹, Sarah W.M. George ², Alexandra Alvarado ³

¹ Institut für Geowissenschaften, Universität Potsdam, 14469 Potsdam, Germany.

² Department of Geosciences, University of Arizona, Tucson, AZ 85721, USA.

³ Instituto Geofísico, Escuela Politécnica Nacional, Quito 170525, Ecuador.

Corresponding author: Audrey Margirier (audrey.margirier@unil.ch)

* Now at the Institute of Earth Surface Dynamics, University of Lausanne, 1015 Lausanne, Switzerland.

Key Points:

- Thermochronological data reveal two cooling phases in the Western Cordillera: one during the Miocene, and one since 6 Ma.
- The onset of cooling at 6 Ma is associated with the onset of active shortening, rock uplift and exhumation in the Western Cordillera.

- The onset of exhumation at 6 Ma was triggered by the initial subduction of the Carnegie Ridge that caused stronger plate coupling.

Abstract

Cenozoic growth of the Andes has been strongly influenced by subduction dynamics, reactivation of inherited crustal heterogeneities, and the superposed effects of climate. Subduction of the submarine Carnegie Ridge has fundamentally impacted late Cenozoic magmatism and tectonic activity in the northern Andes. Time-temperature inverse modeling of new thermochronological data from the Western Cordillera of Ecuador reveals two phases of cooling separated by isothermal conditions. The first cooling phase immediately postdates early and middle Miocene magmatism in the Western Cordillera and is attributed to post-magmatic thermal relaxation. The second cooling phase started after 6 Ma, which we infer to record the onset of exhumation in the Western Cordillera, coeval with the last cooling phase in the Eastern Cordillera. Based on these findings we posit that the onset of subduction of the Carnegie Ridge at \sim 6-5 Ma increased plate coupling at the subduction interface and promoted shortening and regional rock uplift in the northern Andes. Overall, our results highlight the essential role of bathymetric anomalies in driving regional upper-plate deformation at non-collisional convergent plate margins.

Plain language summary

Topographic growth and morphology of the Andes have been strongly influenced by subduction processes, tectonic inheritance, and climate. Here, we investigate the role of subduction of bathymetric highs in driving continental plate deformation at ocean-continent plate margins. The subduction of the Carnegie Ridge, a linear bathymetric high on the subducting Nazca Plate in the Eastern Pacific, has strongly impacted magmatism and tectonic activity in the Ecuadorian Andes. We employed radioisotopic dating techniques and numerical modeling to evaluate the uplift of Andes by exploiting information contained in certain minerals that record the cooling of rock as mountain ranges are uplifted, and eroded. The cooling histories of rocks from the Western Cordillera in Ecuador reveal two distinct phases of cooling. The first phase of cooling occurred shortly after magmatic bodies were emplaced in the Western Cordillera. The second phase began after 6 Ma, which we attribute to the onset of uplift and erosion in the Western Cordillera, coeval with the last cooling phase in the Eastern Cordillera. Based on these findings we suggest that the onset of subduction of the Carnegie Ridge increased the coupling between the two plates and promoted shortening and regional rock uplift in this part of the Andes.

1 Introduction

The topography and morphology of the Andes results from crustal shortening and thickening associated with the convergence of the oceanic Nazca Plate and the continental South American Plate as well as superposed climate-driven surface processes. At the orogen-scale, slab geometry, inherited heterogeneities, and lithospheric strength exert first-order controls on deformation, uplift, and magmatic processes, and thus topography of the upper plate (e.g., Isacks, 1988; Horton and Fuentes, 2016; Rodriguez Piceda et al., 2022). At a more regional scale, the presence of bathymetric highs on the downgoing Nazca Plate also influences the tectono-magmatic and topographic evolution the overriding plate (e.g., Barberi et al., 1988; Espurt et al., 2007; Wipf et al., 2008; Georgieva et al., 2016). Several field studies relate Quaternary coastal uplift, documented by uplifted marine terraces, to the subduction of bathymetric highs such as sea mounts or aseismic ridges (e.g., Macharé and Ortlieb, 1992; Gardner et al., 1992; Hsu, 1992; Padoja et al., 2006; Saillard et al., 2011; Freisleben et al., 2021). On larger spatial scales, long-wavelength uplift of the Amazonian foreland is thought to reflect basal shear and thickening of the lower crust associated with the subduction of the Nazca Ridge underneath the Central Andes (e.g., Espurt et al., 2010; Bishop et al., 2018). Modeling studies suggest that subduction of bathymetric highs enhances upper-plate deformation and promotes regional uplift that propagates away from the trench when the subduction of a ridge initiates (e.g., Dominguez et al., 2000; Gerya et al., 2009; Martinod et al., 2013). While the influence of aseismic ridge subduction in the topographically low forearc and foreland regions is reasonably well documented, the influence of ridge subduction on the high-elevation regions of the northern Andes has remained uncertain. Some authors suggest that the subduction

of the Nazca Ridge and subsequent slab flattening triggered regional uplift in the Western Cordillera and the Subandes of northern Peru (e.g., Margirier et al., 2015; Bishop et al., 2018), but the relative importance of ridge subduction versus the change in slab geometry is unknown. Other studies relate uplift and exhumation of the Eastern Cordillera in Ecuador and Colombia to ridge subduction (Spikings et al., 2001, 2010; Spikings and Simpson, 2014); however, owing to shortening phases unrelated to ridge subduction in the eastern side of the Andes (e.g., Mégard, 1984; Sébrier et al., 1988), the link between exhumation in this area and ridge subduction is not straightforward.

The oblique subduction of the aseismic Carnegie Ridge in Ecuador (Fig. 1) has strongly impacted the geological evolution of the northern Andes by promoting strike-slip faulting and the northward motion of the North Andean Sliver, reactivating inherited tectonic structures (e.g., Egbue and Kellog, 2010; Schütt and Whipp, 2020), and driving changes in magmatism (e.g., Barberi et al., 1988; Bourdon et al., 2003; Chiaradia et al., 2020). Despite its importance for the evolution of the northern Andes, neither the timing of ridge subduction nor its potential impact on uplift and exhumation are well constrained. To unravel these relationships, we present new geochronological and thermochronological data from the previously sparsely dated Western Cordillera integrated with structural information (e.g., Daly, 1989; Eguez et al., 2003), geochemistry (e.g., Bourdon et al., 2003; George et al., 2020), and existing thermochronological data (Spikings et al., 2000, 2001, 2004, 2010; Winkler et al., 2005) to decipher the effect of the onset of ridge subduction, its timing, and the spatiotemporal patterns of exhumation above the subducted portions of the Carnegie Ridge.

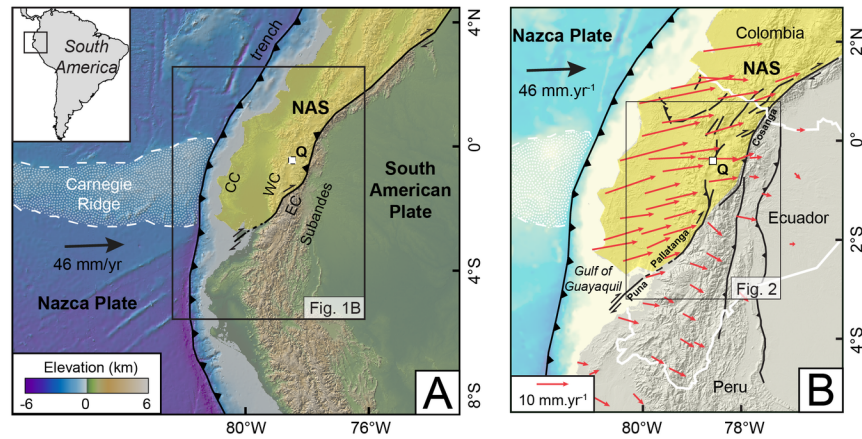


Figure 1. a) Geodynamic setting and topography of the Ecuadorian Andes with bathymetry and Carnegie Ridge. The North Andean Sliver (NAS) is highlighted in yellow. The inset shows the location of study area. b) Active faults (Alvarado et al., 2016; black lines) and GPS horizontal velocity field (red arrows) with respect to stable South America (Nocquet et al., 2014).

2 Geologic and geodynamic setting

2.1 Cenozoic tectonics and exhumation history of the Ecuadorian Andes

The Ecuadorian Andes constitute a bivergent orogen with active thrusting at the western flank of the Western Cordillera (Eguez et al., 2003; Jaillard et al., 2004; Jaillard et al., 2005) and in the Subandes in the east (Baby et al., 2013). Currently, transpression dominates this region, which causes the northward extrusion of the North Andean Sliver along the dextral Puna-Pallatanga-Cosanga fault system (e.g., Alvarado et al., 2016).

The Western and Eastern cordilleras are separated by the Interandean Valley (Fig. 2), which is filled with Cenozoic volcanic and sedimentary rocks (e.g., Hungerbühler et al., 2002). The Western Cordillera is

characterized by a high-elevation (3500 m), low-relief surface capped by Quaternary volcano-sedimentary deposits and Quaternary volcanoes. The western flank of the Western Cordillera is incised by ~2-km-deep valleys exposing Oligocene and Miocene intrusions (31 to 7 Ma; Schütte et al., 2010) and Cretaceous and Paleogene volcano-sedimentary rocks. None of the existing thermochronological data (e.g., Spikings et al., 2005; Winkler et al., 2005; Fig. 2A) has resolved the most recent exhumation history of the Western Cordillera that was associated with topographic growth and valley incision on its western flank. Thermochronological data from the Western and Eastern cordilleras record cooling phases at ~65-55 and 43-30 Ma that were associated with Cenozoic accretion events and changes in plate kinematics that led to exhumation (e.g., Spikings et al., 2001). Thermochronological data from the Eastern Cordillera also record several exhumation phases from 15 Ma to the present that have been linked to the onset of ridge subduction and the subduction of a bathymetric high along the subducting ridge (Spikings et al., 2000; 2001; 2004; 2010).

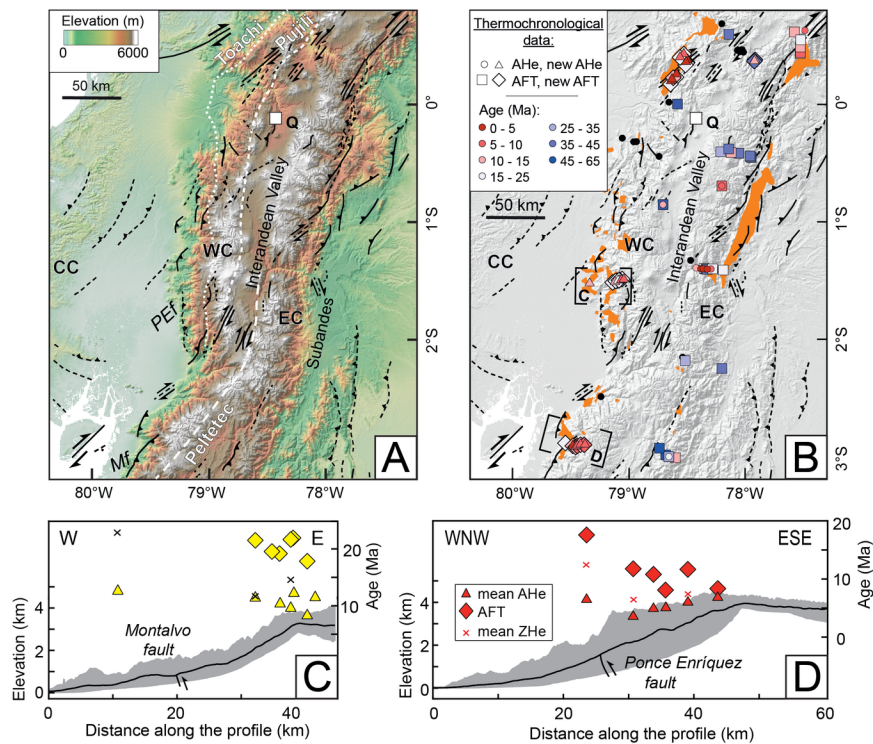


Figure 2. a) Topographic map showing faults (black lines; Eguez et al., 2003), and purported sutures zones (white dashed lines; Alvarado et al., 2014). The Coastal Cordillera (CC), the Western Cordillera (WC) and the Eastern Cordillera (EC) are indicated on the map as well as the Montalvo fault (Mf) and the Ponce Enríquez fault (PEf). b) Existing, and new thermochronological data of the Ecuadorian Andes (non-reset AHe and AFT ages and volcanism ages indicated by black dots; Spikings et al., 2000, 2001, 2004, 2010; Winkler et al., 2005); intrusions (orange) and faults. c, d) Swath profiles across the Montalvo and the Ponce Enríquez reverse faults, respectively and thermochronological ages (Garanda and Cuenca profiles).

2.2 Subduction of the Carnegie Ridge

The aseismic Carnegie Ridge is 200 km wide and rises up to 2 km above the surrounding ocean floor (Fig. 1); it is one of the most prominent bathymetric highs intercepting the South American trench. The oblique subduction of the Carnegie Ridge in Ecuador (Fig. 1) is linked with coastal surface and rock uplift (Pedoja et al., 2006), strike-slip faulting (Fig. 2; e.g., Egbue and Kellogg, 2010; Baize et al., 2015; Alvarado et al., 2016),

changes in magmatism, and the extrusion of the North Andean Sliver coeval with the opening of the Gulf of Guayaquil. However, the timing of onset of Carnegie Ridge subduction is controversial. Spikings et al. (2000, 2001, 2004) suggested an early onset of ridge subduction at 15-10 Ma based on the exhumation history of the Eastern Cordillera. Pilger (1984) suggested that the ridge collided at 15 Ma based on a plate-kinematic reconstruction. Using a refined plate-kinematic reconstruction, Daly (1989) suggested a late Miocene (~ 8 Ma) onset of ridge subduction, which was thought to be in agreement with the timing of arc widening and migration (e.g., Gutscher et al., 1999). Studies based on the timing of submarine canyon incision, marine terrace uplift, and variation in the spatial distribution and chemistry of magmatism have proposed an onset at ~ 5 Ma (Barberi et al., 1988; Collot et al., 2019; Pedoja et al., 2006; Bourdon et al., 2003). Finally, a Pleistocene onset of ridge subduction was suggested based on plate-kinematic reconstructions (Londsdale and Klitgord, 1978), a shift toward adakitic arc volcanics at 1.5 Ma (Samaniego et al., 2005), coastal uplift and stratigraphy of marine terraces (Cantalamessa and Di Celma, 2004), and accelerated subsidence and sedimentation rates in the Gulf of Guayaquil. The latter process was associated with accelerated escape of the North Andean Sliver and the geometry of shelf depocenters (e.g., Witt et al., 2006; Hernández et al., 2020).

3 Methods

Low-temperature thermochronology records the thermal history of the crust that can be related to exhumation and/or cooling/heating events. Exhumation can be, with supporting geological information, interpreted as the combined result of rock uplift and erosion. Zircon (U-Th)/He (ZHe), apatite fission track (AFT) and apatite (U-Th)/He (AHe) thermochronometers are sensitive to temperatures ranging from 200 to 20 °C (e.g., Ault et al., 2019). The thermal histories of Cuenca, Guaranda and Apuela regions in the Western Cordillera were determined using QTQt software, which inverts AFT annealing and AHe diffusion parameters for samples with an elevation relationship (Gallagher, 2012). We used zircon U-Pb geochronology conducted at the Arizona LaserChron Center and published data (Schütte et al., 2010) to determine the crystallization ages of intrusions and as a constraint for thermal modeling. Additional methodological details can be found in Supplemental Data (Text S1; Tables S1, S2).

4 Results

4.1 Zircon U-Pb dating

We obtained 5 new zircon U-Pb ages for the intrusions of the Western Cordillera ranging from 23.9 ± 0.7 to 15.4 ± 0.5 Ma (Fig. 3A; Table 1; Fig. S1). Zircon U-Pb ages from the Apuela Nanegal intrusion in northern Ecuador are 23.9 ± 0.7 (987 m) and 15.4 ± 0.5 Ma (1676 m). In central Ecuador the zircon U-Pb age of the Telimba Chazo Juan intrusion is 21 ± 0.6 Ma (2086 m). In southern Ecuador the zircon U-Pb ages for the Gaby-Papa Grande intrusion and the Chaucha intrusion are 22.7 ± 0.5 Ma (683 m) and 16.9 ± 0.4 Ma (2578 m), respectively.

4.2 Low-temperature thermochronology

We sampled along two structural cross-sections in the central (Guaranda area) and southern parts (Cuenca area) of the Western Cordillera (Fig. 2B, C), spanning an elevation range between 0.9 and 1.4 km. Each transect includes a vertical profile in the hanging wall of the principal reverse fault. We also sampled along a vertical profile in the northern part of the Western Cordillera (Apuela area).

We present 86 AHe single-grain ages for 22 samples, AFT data for 20 samples, and 26 ZHe single-grain ages for 9 samples (Fig. 3; Tables 2, 3, 4; Figs. S2-S7; Tables S3-S24). AHe ages range from 15.4 ± 0.3 to 2.3 ± 0.1 Ma, AFT ages range from 21.7 ± 1.6 to 8.1 ± 1.3 Ma; mean-track lengths are between 13 and 16 μm . For the same samples ZHe ages are younger than AFT ages and range from 23.6 ± 0.3 to 5.9 ± 0.1 Ma (Fig. 3).

Thermochronological ages from the Guaranda cross-section are different either side of the Montalvo reverse fault, with mean AHe and ZHe ages being older in the footwall and younger in the hanging wall (Fig. 2B). AFT dates cluster at 20 Ma in the hanging wall and no AFT date is available in the footwall (Fig. 2B).

Thermochronological ages from the Cuenca cross-section record a clear pattern with older AHe, AFT and ZHe ages for the samples located in the footwall of the Ponce Enríquez reverse fault and younger ages in the hanging wall (Fig. 2C).

Combined, the samples from the vertical profiles cover an elevation range from 950 to 3100 m (Fig. 3). Early Miocene AFT ages from the Apuela and Garanda areas are similar to the ages of intrusion (Fig. 3A, B). In the Cuenca area AFT ages cluster at ~ 11 Ma, and are largely invariant with elevation (Fig. 3C). AHe ages from the different sampling sites are consistent along the Western Cordillera and show an age-elevation relationship, with a trend toward younger ages at lower elevations (Fig. 3D, E, F). AHe ages from the Cuenca and Apuela area clearly show a positive age-elevation relationship (Fig. 3D, F), with ages ranging from 8.7 ± 0.1 Ma to 2.3 ± 0.1 Ma. AHe ages from the Garanda area show more intersample grain-age dispersion and do not reveal such a clear trend with elevation (Fig. 3E). Here, most samples are located at higher elevation, and AHe ages are dispersed around 12 Ma. ZHe ages increase with elevation at the scale of the Western Cordillera.

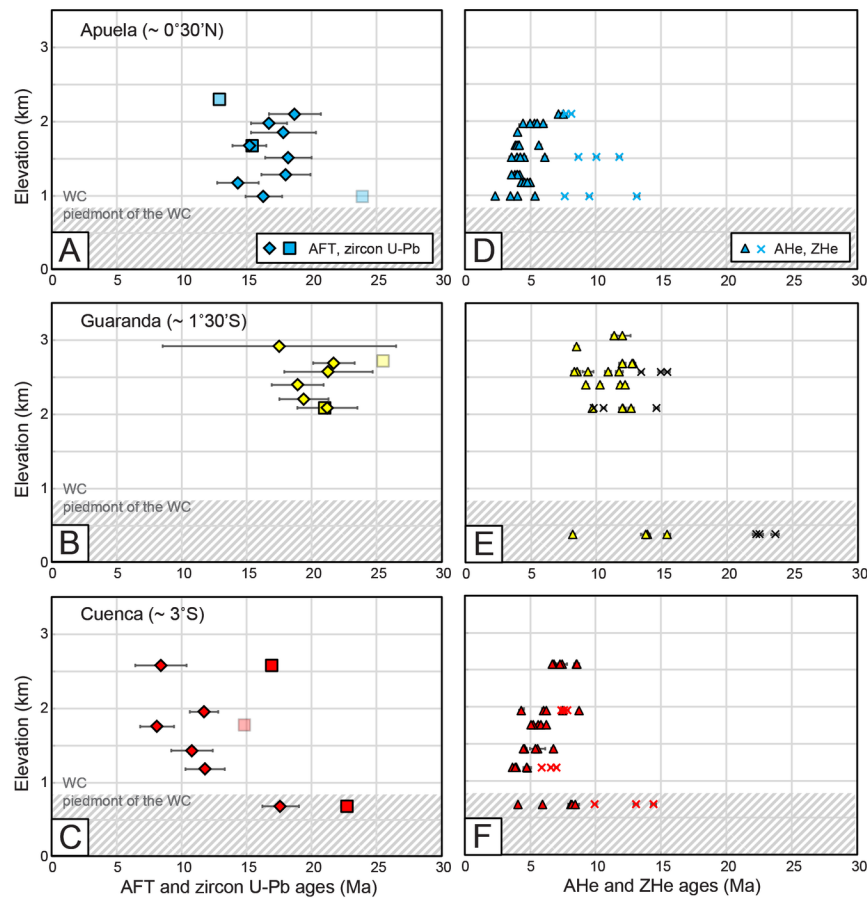


Figure 3. a-c: New AFT ages and zircon U-Pb ages (data from Schütte et al., 2010 are indicated in pastel colors) from the Western Cordillera (WC) plotted against sample elevation for the Apuela, the Guaranda and the Cuenca profiles. d-f: New AHe and ZHe ages from the Western Cordillera plotted against sample elevation for the Apuela, the Guaranda and the Cuenca profiles.

4.3 Thermal modeling

Thermal histories predicted by QTQt satisfactorily reproduced AHe and AFT data for each profile (Fig. 4). The ZHe thermochronometer has a wide range of temperature sensitivity depending on the radiation damage of the zircons (e.g., Ault et al., 2019). As our ZHe data show no clear correlation between the single-grain ages and eU (Figs. S5-S7), we were not able to reproduce the measured ZHe ages with the diffusion model included in QTQt (i.e., Guenther et al., 2013); thus the ZHe data were excluded from the thermal modeling.

The thermal histories that best predict the AHe and AFT data from inversion of the three age-elevation profiles indicate rapid cooling immediately after the emplacement of intrusions ($\sim 100^\circ\text{C}/\text{Myr}$); this was followed by residence of the samples at temperatures of $\sim 100^\circ\text{C}$ from 15 to 6 Ma and from 11 to 6 Ma, for the northern and the southern profiles, respectively. The final cooling phase of the overall thermal history initiated between ~ 6 and 5 Ma, and continues to the present-day ($\sim 15^\circ\text{C}/\text{Myr}$). Although the Garanda profile exhibits a similar early cooling history, the older, high-elevation AHe ages cannot resolve the late Miocene cooling history.

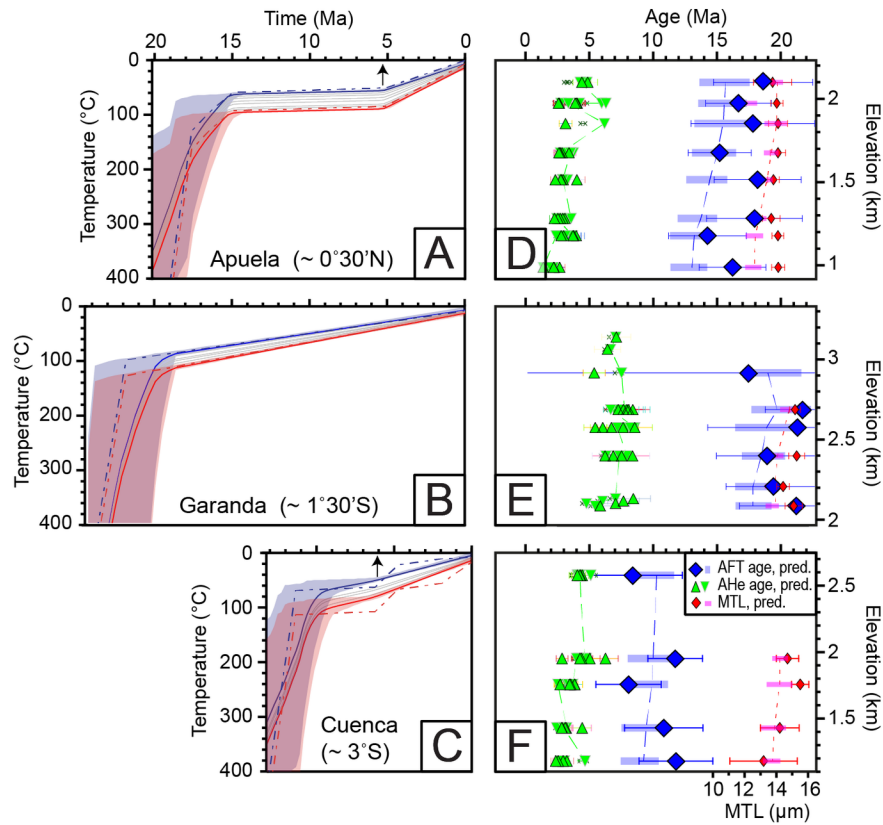


Figure 4. a-c: t-T path for each profile. Each line represents the t-T path of a sample, the red and blue lines represent the t-T path of the lower and upper sample respectively; transparent shading indicates uncertainties. The red and blue dashed lines denote thermal paths that best fit the data. d-f: Age-elevation profiles for the Apuela, Garanda and Cuenca areas showing AFT ages, mean-track length (MTL) and AHe ages; ages predicted based on thermal history are shown by pastel colors.

5. Discussion

5.1 Late Miocene rock uplift and exhumation in the western Ecuadorian Andes

Thermochronological and geochronological data from the Western Cordillera indicate rapid cooling after the

early Miocene crystallization of the intrusions (Fig. 4). Initial early Miocene rapid cooling likely corresponds to post-magmatic cooling via thermal relaxation of the intrusions (e.g., Murray et al., 2019), although coeval exhumation cannot be excluded. The most recent cooling histories documented by the Cuenca and the Apuela profiles are consistent and record an isothermal phase followed by a second cooling phase starting at ~ 6 -5 Ma. The isothermal phase suggests that little exhumation occurred in the Western Cordillera between 15 and 6-5 Ma. The second cooling phase in the Western Cordillera is synchronous with the onset of the last cooling phase recorded in the Eastern Cordillera (starting at 5.5 Ma; Spikings and Crowhurst, 2004; Spikings et al., 2010), and with rapid cooling in the Coastal Cordillera between 6 and 5 Ma (Brichau et al., 2021). This late Miocene cooling in both cordilleras is also contemporaneous with the formation of alluvial-fan deposition in the basins to the west and east of the Andes (e.g., Alvarado et al., 2016), supporting the idea that this cooling phase was associated with erosional exhumation. The cooling rate and the geothermal gradient of $30^{\circ}\text{C}/\text{km}$ derived from the modeling of our thermochronological data suggest exhumation rates of $\sim 0.5 \text{ km}/\text{Myr}$ for the last 6 Myr, with total exhumation of $\sim 3 \text{ km}$ achieved since 6 Ma.

In contrast to the simple two-stage cooling history of the Western Cordillera, previous thermochronological studies from the Eastern Cordillera and the Coastal Cordillera have suggested multiple phases of exhumation starting at 15, 9, and 6 Ma, and starting at 6 and 2 Ma, respectively (Spikings et al. 2010; Brichau et al., 2021). AFT data from the Interandean Cuenca Basin suggest that it experienced a cooling history similar to the Eastern Cordillera, including a major cooling event at 9 Ma accompanied by shortening (Steinmann et al., 1999). The AHe ages along the Garanda and Cuenca cross-sections are younger in the hanging wall of the reverse faults, whereas they are older in both the footwall and at high elevations in the hanging wall (Fig. 2B, C). This AHe age pattern suggests uplift of the hanging walls of the Montalvo and Ponce Enrquez reverse faults and internal deformation of the North Andean Sliver. Together with thermal histories obtained for vertical profiles (Fig. 4), the spatial age patterns suggest that shortening along these faults controlled uplift and exhumation in the Western Cordillera during the late Miocene synchronous with shear-zone reactivation in the Western Cordillera (Spikings et al., 2005), and deformation and exhumation along the Eastern Cordillera and the Subandes (Spikings and Crowhurst, 2004; Spikings et al., 2010).

Coltorti et al. (2000) suggested that an extensive low-relief surface in the Western Cordillera at 3500 m was at sea level during the early Pliocene ($\sim 5.3 \text{ Ma}$) but became dissected because of uplift in the middle and late Pliocene. In light of our new thermochronological data these observations suggest that cooling in the Western Cordillera involving a total of 3 km of exhumation must have been associated with rock and surface uplift starting at $\sim 6 \text{ Ma}$. In southern Ecuador a low surface elevation in the Western Cordillera prior to 6 Ma is compatible with marine sediments in the inter-Andean basins deposited between 15 and 9 Ma (Steinmann et al., 1999; Hungerbhler et al., 2002). Finally, the combination of sedimentological and thermochronological data from the Western Cordillera and the Eastern Cordillera (i.e., Winkler et al., 2005) suggests limited structural uplift in the Western Cordillera prior to 6 Ma. Thus, the present-day topography of the Ecuadorian Andes, including two parallel, high-elevation mountain ranges separated by an intermontane depression, must have initiated at $\sim 6 \text{ Ma}$.

5.2 Implications for the timing of Carnegie Ridge subduction

The subduction of bathymetric highs has been suggested to trigger widespread deformation and uplift in non-collisional orogens (e.g., Lallemand et al., 1992; von Huene et al., 1997; Dominguez et al., 1998; Pubellier et al., 1999; Ramos, 2005; Martinod et al., 2013; Spikings and Simpson, 2014; Georgieva et al., 2016) and island arcs (Taylor et al., 1987; Mann et al., 1998; Rosenbaum and Mo, 2011; Freisleben et al., 2021). In addition, the subduction of oceanic aseismic ridges also appears to cause changes in the geochemical composition of magmatism with a shift to a more juvenile isotope signal (Chiaradia et al., 2020). Our thermochronological data from the Western Cordillera in Ecuador clearly document the onset of a regional uplift and exhumation phase that started at ~ 6 -5 Ma (Fig. 4). Our data suggest that the Ponce Enrquez and Montalvo reverse faults are major structures controlling rock uplift and exhumation in the Western Cordillera. Importantly, these faults appear to be associated with transpression and the extrusion of the North Andean Sliver along the dextral Puna-Pallatanga-Cosanga strike-slip fault. Although the North Andean Sliver may have initiated as

early as 15 Ma due to oblique subduction (e.g., Alvarado et al., 2016), the acceleration of northward motion of this block suggests increased coupling at the plate interface after the interception of the Carnegie Ridge (Witt et al., 2006). Importantly, earlier cooling and exhumation phases identified in the Eastern Cordillera and the Coastal Cordillera between 15 and 7 Ma (Spikings et al., 2005, 2010; Brichau et al., 2021) that have been associated with subduction of the Carnegie Ridge (i.e., Spikings et al., 2010), were synchronous with deformation and uplift recorded at 17-15 Ma, 13 Ma, and 9-8 Ma in the sub-Andes of northern Peru (e.g., Mégard, 1984; Sébrier et al., 1988; Moreno et al., 2020). These earlier cooling phases, however, are not recorded in the Western Cordillera, suggesting that earlier uplift and exhumation in other parts of Ecuador were independent from aseismic ridge subduction processes.

Initial Carnegie Ridge subduction at \sim 6-5 Ma is consistent with geodynamic reconstructions and with the results of studies of the offshore morphology and subsidence history of the Gulf of Guayaquil that propose an onset of ridge subduction at 5 Ma and document ongoing ridge subduction by \sim 1.8 Ma (e.g., Witt et al., 2006; Collot et al., 2019). Onset of ridge subduction at \sim 6-5 Ma is also compatible with the timing of regional compressional tectonic inversion of the forearc (Daly, 1989). Moreover, an eastward shift of volcanism at 6-5 Ma in northern Ecuador (Barberi et al., 1988) and a subsequent change in magma chemistry also support the notion of onset of Carnegie Ridge subduction at this time (e.g., Bourdon et al., 2003; Samadiego et al., 2010).

Taken together, our thermochronological and geochronological data suggest that the subduction of the Carnegie Ridge triggered shortening and exhumation in the Ecuadorian Andes starting at \sim 6-5 Ma (Fig. 5). However, a delay between the onset of ridge subduction and exhumation processes in the high Andes is possible. Thus, we cannot exclude an onset of Carnegie Ridge subduction at 9-8 Ma as previously suggested by Daly (1989) and Gutscher et al. (1999) based on plate kinematic reconstruction. Finally, Hafnium isotopic compositions of zircons in Ecuador become more juvenile at 8-6 Ma (George et al., 2020) and could also reflect the arrival of the Carnegie Ridge at the trench and ensuing changes in volcanic arc geochemistry at that time.

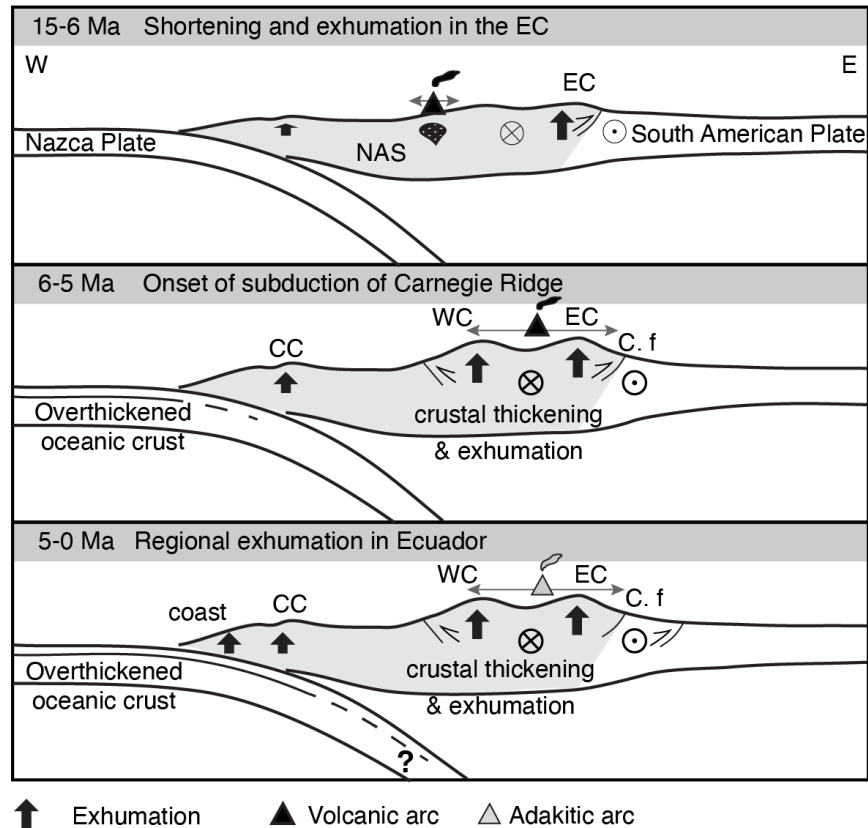


Figure 5: Schematic cross-sections showing tectonic changes and topographic growth in Ecuador (at $\sim 2^\circ\text{S}$) during the late Cenozoic. The North Andean Sliver (NAS) is indicated in grey. The Coastal Cordillera (CC), Western Cordillera (WC) and the Eastern Cordillera (EC) as well as the position of the magmatic arc (after George et al., 2021) are showed on the figure.

6. Conclusions

New geochronological and thermochronological data constrain several cooling phases in the Western Cordillera of Ecuador. AFT ages record cooling associated with post-magmatic thermal relaxation of early and middle Miocene intrusions. This suggests that the AFT thermochronometer is not well suited to decipher the exhumation of the Miocene magmatic arc in the northern Andes. Thermal modeling of our data constrains two cooling phases: a post-magmatic cooling during early and middle Miocene associated with thermal relaxation, a period of tectonic quiescence, and a second phase driven by uplift and exhumation since $\sim 6\text{-}5$ Ma in the Western Cordillera. This latest Miocene onset of exhumation correlates well with the onset of active shortening and rock uplift, as well as coeval exhumation previously identified in the Coastal Cordillera and the Eastern Cordillera of the northern Andes. We propose that the onset of regional shortening and exhumation at $\sim 6\text{-}5$ Ma was triggered by the effects of initial subduction of the Carnegie Ridge that caused stronger plate coupling.

Acknowledgements

This study was supported by a PRIME grant of the German Academic Exchange Service, funds from the Potsdam University Graduate School, and support for the Arizona LaserChron Center (NSF-EAR 1649254). We thank U. Chowdhury and the students for assistance at the ANGL laboratory.

Open research

The data will be deposited in a trusted repository that supports the FAIR principles by the time our article is accepted, the data is available in the supporting information, tables, and figures for the purposes of peer review.

References cited

Alvarado, A., Audin, L., Nocquet, J.-M., Jaillard, E., Mothes, P., Jarrin, P., Segovia, M., Rolandone, F., and Cisneros, D., 2016, Partitioning of oblique convergence in the Northern Andes subduction zone: Migration history and the present-day boundary of the North Andean Sliver in Ecuador: *Tectonics*, v. 35, no. 5, p. 1048-1065, doi: 10.1002/(ISSN)1944-9194.

Ault, A. K., Gautheron, C., & King, G. E., 2019, Innovations in (U–Th)/He, fission track, and trapped charge thermochronometry with applications to earthquakes, weathering, surface-mantle connections, and the growth and decay of mountains. *Tectonics*, v. 38, p. 3705–3739. <https://doi.org/10.1029/2018TC005312>

Baby, P., Rivadeneira, M., Barragán, R., and Christophoul, F., 2013, Thick-skinned tectonics in the Oriente foreland basin of Ecuador: Geological Society, London, Special Publications, v. 377, no. 1, p. 59–76, doi: 10.1785/gssrl.67.6.27.

Baize, S., Audin, L., Winter, T., Alvarado, A., Moreno, L.P., Taibe, M., Reyes, P., Kauffmann, P. and Yepes, H., 2015. Paleoseismology and tectonic geomorphology of the Pallatanga fault (Central Ecuador), a major structure of the South-American crust. *Geomorphology*, v. 237, pp.14-28.

Barberi, F., Coltelli, M., and Ferrara, G., 1988, Plio-quadernary volcanism in Ecuador: *Geological Magazine*, v. 125, no. 1, p. 1-14.

Bishop, B.T., Beck, S.L., Zandt, G., Wagner, L.S., Long, M.D., and Tavera, H., 2018, Accepted Manuscript: *Tectonophysics*, v. 731, p. 73-84, doi: 10.1016/j.tecto.2018.03.005.

Bourdon, E., Eissen, J.-P., Gutscher, M.-A., Monzier, M., Hall, M.L., and Cotten, J., 2003, Magmatic response to early aseismic ridge subduction: the Ecuadorian margin case (South America): *Earth and Planetary Science Letters*, v. 205, no. 3, p. 123–138.

Brichau, S., Reyes, P., Gautheron, C., Hernández, M., Michaud, F., Leisen, M., Vacherat, A., Saillard, M., Proust, J.N., and O’Sullivan, P., 2021, First timing constraints on the Ecuadorian Coastal Cordillera exhumation: geodynamic implications: *Journal of South American Earth Sciences*, v. 105, 103007, p. 1–57.

Cantalamesa, G., and Di Celma, C., 2004, Origin and chronology of Pleistocene marine terraces of Isla de la Plata and of flat, gently dipping surfaces of the southern coast of Cabo San Lorenzo (Manabí, Ecuador): *Journal of South American Earth Sciences*, v. 16, no. 8, p. 633-648.

Chiaradia, M., Müntener, O. and Beate, B., 2020. Effects of aseismic ridge subduction on the geochemistry of frontal arc magmas. *Earth and Planetary Science Letters*, v. 531, 115984.

Collot, J.-Y., Ratzov, G., Silva, P., Proust, J.N., Migeon, S., Hernández, M.J., Michaud, F., Pazmino, A., Barba Castillo, D., Alvarado, A., and Khurama, S., 2019, The Esmeraldas Canyon: A Helpful Marker of the Pliocene-Pleistocene Tectonic Deformation of the North Ecuador-Southwest Colombia Convergent Margin: *Tectonics*, v. 38, no. 8, p. 3140–3166, doi: 10.1190/1.9781560801580.

Coltorti, M., and Ollier, C.D., 2000, Geomorphic and tectonic evolution of the Ecuadorian Andes: *Geomorphology*, v. 32, p. 1–19.

Daly, M.C., 1989, Correlations between Nazca/Farallon Plate kinematics and forearc evolution in Ecuador: *Tectonics*, v. 8, no. 4, p. 769–790.

Dominguez, S., Lallemand, S.E., Malavieille, J., and von Huene, R., 1998, Upper plate deformation associated with seamount subduction: *Tectonophysics*, v. 293, no. 3-4, p. 207-224.

Dominguez, S., Malavieille, J. and Lallemand, S.E., 2000. Deformation of accretionary wedges in response to seamount subduction: Insights from sandbox experiments: *Tectonics* , v. 19 , no. 1, p. 182-196.

Donelick, R.A., 1993. Apatite etching characteristics versus chemical composition. *Nuclear Tracks and Radiation Measurements* ,21 (604), pp.1359-0189.

Egbue, O. and Kellogg, J., 2010. Pleistocene to present North Andean “escape”: *Tectonophysics* , v. 489 , no. 1-4, p. 248-257.

Eguez, A., Alvarado, A., Yepes, H., Machette, M.N., Costa, C., Dart, R.L., and Bradley, L.-A., 2003, Database and Map of Quaternary Faults and Folds of Ecuador and its offshore regions: Open-File Report 03-289, U.S. Geological Survey.

Espurt, N., Baby, P., Brusset, S., Roddaz, M., Hermoza, W., Regard, V., Antoine, P.O., Salas-Gismondi, R., and Bolanos, R., 2007, How does the Nazca Ridge subduction influence the modern Amazonian foreland basin?: *Geology*, v. 35, no. 6, p. 515, doi: 10.1130/G23237A.1.

Espurt, N., Baby, P., Brusset, S., Roddaz, M., Hermoza, W. and Barbarand, J., 2010. The Nazca Ridge and uplift of the Fitzcarrald Arch: implications for regional geology in northern South America. *Amazonia: Landscape and Species Evolution: A Look into the Past*. Wiley-Blackwell , p. 89-100.

Evans, N.J., Byrne, J.P., Keegan, J.T. and Dotter, L.E., 2005, Determination of uranium and thorium in zircon, apatite, and fluorite: Application to laser (U-Th)/He thermochronology: *Journal of Analytical Chemistry*, v. 60, no. 12, p.1159-1165.

Farley, K.A. and Stockli, D.F., 2002, (U-Th)/He dating of phosphates: Apatite, monazite, and xenotime: *Reviews in mineralogy and geochemistry*, v. 48, no. 1, p.559-577.

Flowers, R.M., Ketcham, R.A., Shuster, D.L. and Farley, K.A., 2009. Apatite (U–Th)/He thermochronometry using a radiation damage accumulation and annealing model. *Geochimica et Cosmochimica acta* , 73 (8), pp.2347-2365.

Freisleben, R., Jara-Munoz, J., Melnick, D., Martinez, J. M., and Strecker, M. R., 2021, Marine terraces of the last interglacial period along the Pacific coast of South America (1deg N–40deg S). *Earth System Science Data*, v. 13, no. 6, p. 2487-2513.

Gallagher, K., 2012, Transdimensional inverse thermal history modeling for quantitative thermochronology: *Journal of Geophysical Research*, v. 117, no. B2, p. B02408.

Gardner, T.W., Verdonck, D., Pinter, N.M., Slingerland, R., Furlong, K.P., Bullard, T.F. and Wells, S.G., 1992, Quaternary uplift astride the aseismic Cocos ridge, Pacific coast, Costa Rica: *Geological Society of America Bulletin* , v. 104 , no. 2, p. 219-232.

Gautheron, C., Tassan-Got, L., Barbarand, J. and Pagel, M., 2009. Effect of alpha-damage annealing on apatite (U–Th)/He thermochronology. *Chemical Geology* , 266 (3-4), pp.157-170.

Gehrels, G.E., Valencia, V.A. and Ruiz, J., 2008. Enhanced precision, accuracy, efficiency, and spatial resolution of U-Pb ages by laser ablation–multicollector–inductively coupled plasma–mass spectrometry. *Geochemistry, Geophysics, Geosystems* , 9 (3).

Gehrels, G. and Pecha, M., 2014. Detrital zircon U-Pb geochronology and Hf isotope geochemistry of Paleozoic and Triassic passive margin strata of western North America. *Geosphere* , 10 (1), pp.49-65.

George, S.W.M., Horton, B.K., Vallejo, C., Jackson, L.J., Gabriela Gutierrez, E., 2021, Did accretion of the Caribbean oceanic plateau drive rapid crustal thickening in the northern Andes?: *Geology* , v. 49, no. 8, p. 936-940.

Georgieva, V., Melnick, D., Schildgen, T.F., and Ehlers, T.A., 2016, Tectonic control on rock uplift, exhumation, and topography above an oceanic ridge collision: Southern Patagonian Andes (47degS), Chile:

Tectonics, v. 35, no. 6, 1317-1341.

Gerya, T. V., Fossati, D., Cantieni, C., & Seward, D., 2009, Dynamic effects of aseismic ridge subduction: numerical modelling: *European Journal of Mineralogy*, v. 21, no. 3, p. 649-661.

Ginster, U., Reiners, P.W., Nasdala, L. and Chanmuang, C., 2019. Annealing kinetics of radiation damage in zircon. *Geochimica et Cosmochimica Acta* , 249 , pp.225-246.

Guenther, W.R., Reiners, P.W., Ketcham, R.A., Nasdala, L. and Giester, G., 2013, Helium diffusion in natural zircon: Radiation damage, anisotropy, and the interpretation of zircon (U-Th)/He thermochronology: *American Journal of Science* , v. 313 , no. 3, p. 145-198.

Gutscher, M.A., Malavieille, J., Lallemand, S., and Collot, J.-Y., 1999, Tectonic segmentation of the North Andean margin: impact of the Carnegie Ridge collision: *Earth and Planetary Science Letters*, v. 168, no. 3, p. 255–270.

Hernandez, M. J., Michaud, F., Collot, J. Y., Proust, J. N., & d’Acremont, E., 2020, Evolution of the Ecuador offshore nonaccretionary-type forearc basin and margin segmentation: *Tectonophysics*, v. 781, 228374.

Horton, B.K., and Fuentes, F., 2016, Sedimentary record of plate coupling and decoupling during growth of the Andes: *Geology*, v. 44, no. 8, p. 647–650.

Hsu, J.T., 1992, Quaternary uplift of the Peruvian coast related to the subduction of the Nazca Ridge: 13.5 to 15.6 degrees south latitude: *Quaternary International* , v. 15 , p. 87-97.

Hungerbuhler, D., M. Steinmann, W. Winkler, D. Seward, A. Eguez, D. E. Peterson, U. Helg, and C. Hammer, 2002, Neogene stratigraphy and Andean geodynamics of southern Ecuador: *Earth-Science Reviews*, v. 57, no. 1-2, p. 75-124.

Hurford, A.J. and Green, P.F., 1982, A users’ guide to fission track dating calibration. *Earth and Planetary Science Letters* , v.59 , no. 2, p.343-354.

Isacks, B.L., 1988, Uplift of the central Andean plateau and bending of the Bolivian orocline: *Journal of Geophysical Research: Solid Earth (1978–2012)*, v. 93, no. B4, p. 3211–3231.

Jaillard, E., Ordonez, M., Suarez, J., Toro, J., Iza, D., and Lugo, W., 2004, Stratigraphy of the late Cretaceous–Paleogene deposits of the Cordillera Occidental of central Ecuador: geodynamic implications, *Journal of South American Earth Sciences* , v. 17 , no. 1, p. 49-58.

Jaillard, E., Guillier, B., Bonnardot, M.-A., Hassani, R., Lapierre, H., and Toro, J., 2005, Orogenic buildup of the Ecuadorian Andes, *6th International Symposium on Andean Geodynamics (Barcelona)* , extended abstract, p. 404-407.

Ketcham, R.A., Carter, A., Donelick, R.A., Barbarand, J. and Hurford, A.J., 2007. Improved modeling of fission-track annealing in apatite. *American Mineralogist* , 92 (5-6), pp.799-810.

Ketcham, R.A., Gautheron, C. and Tassan-Got, L., 2011. Accounting for long alpha-particle stopping distances in (U–Th–Sm)/He geochronology: Refinement of the baseline case: *Geochimica et Cosmochimica Acta*, v. 75, no. 24, p.7779-7791.

Lallemand, S. E., Malavieille, J., and Calassou, S., 1992, Effects of oceanic ridge subduction on accretionary wedges: experimental modeling and marine observations: *Tectonics* , v. 11 , no. 6, p. 1301-1313.

Laslett, G.M., Galbraith, R.F. and Green, P.F., 1994, The analysis of projected fission track lengths: *Radiation measurements* , v.23 , no. 1, p.103-123.

Lonsdale, P., and Klitgord, K.D., 1978, Structure and tectonic history of the eastern Panama Basin: *Geological Society of America Bulletin* , v. 89 , no. 7, p. 981-999.

Ludwig, K.R., 2008. User's Manual for Isoplot 3.6 4. *Berkeley Geochronology Center Special Publication* , p.78.

Machare, J. and Ortlieb, L., 1992, Plio-Quaternary vertical motions and the subduction of the Nazca Ridge, central coast of Peru: *Tectonophysics* , v. 205 , no. 1-3, p. 97-108.

Mann, P., Taylor, F.W., Lagoe, M.B., Quarles, A. and Burr, G., 1998, Accelerating late Quaternary uplift of the New Georgia Island Group (Solomon island arc) in response to subduction of the recently active Woodlark spreading center and Coleman seamount: *Tectonophysics*, v. 295, no. 3-4, p. 259-306.

Margirier, A., Robert, X., Audin, L., Gautheron, C., Bernet, M., Hall, S., and Simon-Labric, T., 2015, Slab flattening, magmatism, and surface uplift in the Cordillera Occidental (northern Peru): *Geology*, v. 43, no. 11, p. 1031–1034.

Martinod, J., Guillaume, B., Espurt, N., and Faccenna, C., 2013, Effect of aseismic ridge subduction on slab geometry and overriding plate deformation: Insights from analogue modeling: *Tectonophysics*, v. 588, p. 39-55.

Megard, F., 1984, The Andean orogenic period and its major structures in central and northern Peru: *Journal of the Geological Society* ,141 (5), 893-900.

Michaud, F., Witt, C., and Royer, J.-Y., 2009, Influence of the subduction of the Carnegie volcanic ridge on Ecuadorian geology: Reality and fiction: *Geological Society of America Memoirs*, v. 204, no. 0, p. 217–228, doi: 10.1130/2009.1204(10).

Moreno, F., Garzzone, C.N., George, S.W., Horton, B.K., Williams, L., Jackson, L.J., Carlotto, V., Richter, F. and Bandeian, A., 2020, Coupled Andean growth and foreland basin evolution, Campanian–Cenozoic Bagua Basin, northern Peru: *Tectonics*, v. 39, no. 7, p.e2019TC005967.

Murray, K.E., Reiners, P.W., Thomson, S.N., Robert, X. and Whipple, K.X., 2019, The thermochronologic record of erosion and magmatism in the Canyonlands region of the Colorado Plateau: *American journal of science*, v. 319, no. 5, p.339–380.

Pedoja, K., Dumont, J.F., Lamothe, M., Ortlieb, L., Collot, J.-Y., Ghaleb, B., Auclair, M., Alvarez, V., and Labrousse, B., 2006, Plio-Quaternary uplift of the Manta Peninsula and La Plata Island and the subduction of the Carnegie Ridge, central coast of Ecuador: *Journal of South American Earth Sciences*, v. 22, no. 1-2, p. 1–21, doi: 10.1016/j.jsames.2006.08.003.

Pilger, R.H., 1984, Cenozoic plate kinematics, subduction and magmatism: South American Andes: *Journal of the Geological Society* , v.141 , no. 5, p. 793-802.

Pubellier, M., Bader, A. G., Rangin, C., Deffontaines, B., and Quebral, R., 1999, Upper plate deformation induced by subduction of a volcanic arc: the Snellius Plateau (Molucca Sea, Indonesia and Mindanao, Philippines): *Tectonophysics* , v. 304 , no. 4, p. 345-368.

Pullen, A., Ibanez-Mejia, M., Gehrels, G.E., Giesler, D. and Pecha, M., 2018. Optimization of a laser ablation-single collector-inductively coupled plasma-mass spectrometer (Thermo Element 2) for accurate, precise, and efficient zircon U-Th-Pb geochronology. *Geochemistry, Geophysics, Geosystems* , 19 (10), pp.3689-3705.

Ramos, V.A., 2005, Seismic ridge subduction and topography: Foreland deformation in the Patagonian Andes: *Tectonophysics*, v. 399, no. 1-4, p. 73–86, doi: 10.1016/j.tecto.2004.12.016.

Reiners, P.W., Spell, T.L., Nicolescu, S. and Zanetti, K.A., 2004, Zircon (U-Th)/He thermochronometry: He diffusion and comparisons with ⁴⁰Ar/³⁹Ar dating: *Geochimica et cosmochimica acta*, v. 68, no. 8, p.1857-1887.

Rodriguez Picada, C., Scheck-Wenderoth, M., Cacace, M., Bott, J., & Strecker, M. R. (2022). Long-term lithospheric strength and upper-plate seismicity in the southern Central Andes, 29deg–39degS. *Geochemistry*,

Geophysics, Geosystems, v. 23, e2021GC010171.

Rosenbaum, G. and Mo, W., 2011. Tectonic and magmatic responses to the subduction of high bathymetric relief. *Gondwana Research*, v. 19, no. 3, p. 571-582.

Saillard, M., Hall, S.R., Audin, L., Farber, D.L., Regard, V. and Hérail, G., 2011, Andean coastal uplift and active tectonics in southern Peru: ^{10}Be surface exposure dating of differentially uplifted marine terrace sequences (San Juan de Marcona, $\sim 15.4^\circ\text{S}$): *Geomorphology*, v. 128, no. 3-4, p. 178-190.

Samaniego, P., Martin, H., Monzier, M., Robin, C., Fornari, M., Eissen, J. P., & Cotten, J., 2005, Temporal evolution of magmatism in the Northern Volcanic Zone of the Andes: the geology and petrology of Cayambe Volcanic Complex (Ecuador): *Journal of petrology*, v. 46, no. 11, p. 2225-2252.

Schütt, J.M., and Whipp, D.M., 2020, Controls on Continental Strain Partitioning Above an Oblique Subduction Zone, Northern Andes: *Tectonics*, v. 39, no. 4, p. 725, doi: 10.1002/2015TC003941.

Schütte, P., Chiaradia, M., and Beate, B., 2010, Geodynamic controls on Tertiary arc magmatism in Ecuador: Constraints from U–Pb zircon geochronology of Oligocene–Miocene intrusions and regional age distribution trends: *Tectonophysics*, v. 489, no. 1-4, p. 159–176, doi: 10.1016/j.tecto.2010.04.015.

Sébrier, M., Mercier, J.L., Macharé, J., Bonnot, D., Cabrera, J., and Blanc, J.L., 1988, The state of stress in an overriding plate situated above a flat slab: The Andes of central Peru: *Tectonics*, v. 7, no. 4, p. 895-928.

Spikings, R.A., and Crowhurst, P.V., 2004, (U-Th)/He thermochronometric constraints on the late Miocene–Pliocene tectonic development of the northern Cordillera Real and the Interandean Depression, Ecuador: *Journal of South American Earth Sciences*, v. 17, no. 4, p. 239–251.

Spikings, R., and Simpson, G., 2014, Rock uplift and exhumation of continental margins by the collision, accretion, and subduction of buoyant and topographically prominent oceanic crust: *Tectonics*, v. 33, no. 5, p. 635-655.

Spikings, R.A., Crowhurst, P.V., Winkler, W., and Villagomez, D., 2010, Syn- and post-accretionary cooling history of the Ecuadorian Andes constrained by their in-situ and detrital thermochronometric record: *Journal of South American Earth Sciences*, v. 30, no. 3-4, p. 121–133, doi: 10.1016/j.jsames.2010.04.002.

Spikings, R.A., Seward, D., Winkler, W., and Ruiz, G.M., 2000, Low-temperature thermochronology of the northern Cordillera Real, Ecuador: Tectonic insights from zircon and apatite fission track analysis: *Tectonics*, v. 19, no. 4, p. 649-668.

Spikings, R.A., Winkler, W., Seward, D., and Handler, R., 2001, Along-strike variations in the thermal and tectonic response of the continental Ecuadorian Andes to the collision with heterogeneous oceanic crust: *Earth and Planetary Science Letters*, v. 186, no. 1, p. 57–73.

Stacey, J.S. and Kramers, J.D., 1975. Approximation of terrestrial lead isotope evolution by a two-stage model: *Earth Planetary Science Letters*, v. 26. doi, 10, pp.90088-6.

Steinmann, M., Hungerbühler, D., Seward, D., and Winkler, W., 1999, Neogene tectonic evolution and exhumation of the southern Ecuadorian Andes: a combined stratigraphy and fission-track approach: *Tectonophysics*, v. 307, p. 255–276.

Taylor, F.W., Fröhlich, C., Lecolle, J., Strecker, M., 1987, Analysis of partially emerged corals and reef terraces in the central Vanuatu Arc: Comparison of contemporary coseismic and nonseismic with quaternary vertical movements: *Journal of Geophysical Research*, v. 92, no. B6, p. 4905. doi:10.1029/JB092iB06p04905.

Von Huene, R., Corvalán, J., Flueh, E. R., Hinz, K., Korstgard, J., Ranero, C. R., and Weinrebe, W., 1997, Tectonic control of the subducting Juan Fernandez Ridge on the Andean margin near Valparaíso, Chile: *Tectonics*, v. 16, no. 3, p. 474-488.

Winkler, W., Villagomez, D., Spikings, R., Abegglen, P., Tobler, S., and Eguez, A., 2005, The Chota basin and its significance for the inception and tectonic setting of the inter-Andean depression in Ecuador: *Journal of South American Earth Sciences*, v. 19, no. 1, p. 5–19, doi: 10.1016/j.jsames.2004.06.006.

Wipf, M., Zeilinger, G., Seward, D. and Schlunegger, F., 2008. Focused subaerial erosion during ridge subduction: Impact on the geomorphology in south-central Peru. *Terra Nova*, v. 20, no. 1, p.1-10.

Witt, C., Bourgois, J., Michaud, F., Ordonez, M., Jimenez, N., and Sosson, M., 2006, Development of the Gulf of Guayaquil (Ecuador) during the Quaternary as an effect of the North Andean block tectonic escape: *Tectonics*, v. 25, no. 3, p. TC3017.

Table 1. Zircon U-Pb from the Western Cordillera (Ecuador).

Table 2. Apatite (U-Th-Sm)/He data from the Western Cordillera (Ecuador).

Table 3. Zircon (U-Th)/He single-grain ages from the Western Cordillera (Ecuador).

Table 4. Apatite fission track data from the Western Cordillera (Ecuador).

Exhumation of the Western Cordillera, Ecuador, driven by late Miocene subduction of the Carnegie Ridge

Audrey Margirier ^{1*}, Manfred R. Strecker ¹, Peter W. Reiners ², Stuart N. Thomson ², Ismael Casado ¹, Sarah W.M. George ², Alexandra Alvarado ³

¹ Institut für Geowissenschaften, Universität Potsdam, 14469 Potsdam, Germany.

² Department of Geosciences, University of Arizona, Tucson, AZ 85721, USA.

³ Instituto Geofísico, Escuela Politécnica Nacional, Quito 170525, Ecuador.

Corresponding author: Audrey Margirier (audrey.margirier@unil.ch)

* Now at the Institute of Earth Surface Dynamics, University of Lausanne, 1015 Lausanne, Switzerland.

Key Points:

- Thermochronological data reveal two cooling phases in the Western Cordillera: one during the Miocene, and one since 6 Ma.
- The onset of cooling at 6 Ma is associated with the onset of active shortening, rock uplift and exhumation in the Western Cordillera.
- The onset of exhumation at 6 Ma was triggered by the initial subduction of the Carnegie Ridge that caused stronger plate coupling.

Abstract

Cenozoic growth of the Andes has been strongly influenced by subduction dynamics, reactivation of inherited crustal heterogeneities, and the superposed effects of climate. Subduction of the submarine Carnegie Ridge has fundamentally impacted late Cenozoic magmatism and tectonic activity in the northern Andes. Time-temperature inverse modeling of new thermochronological data from the Western Cordillera of Ecuador reveals two phases of cooling separated by isothermal conditions. The first cooling phase immediately postdates early and middle Miocene magmatism in the Western Cordillera and is attributed to post-magmatic thermal relaxation. The second cooling phase started after 6 Ma, which we infer to record the onset of exhumation in the Western Cordillera, coeval with the last cooling phase in the Eastern Cordillera. Based on these findings we posit that the onset of subduction of the Carnegie Ridge at ~6-5 Ma increased plate coupling at the subduction interface and promoted shortening and regional rock uplift in the northern Andes. Overall, our results highlight the essential role of bathymetric anomalies in driving regional upper-plate deformation at non-collisional convergent plate margins.

Plain language summary

Topographic growth and morphology of the Andes have been strongly influenced by subduction processes, tectonic inheritance, and climate. Here, we investigate

the role of subduction of bathymetric highs in driving continental plate deformation at ocean-continent plate margins. The subduction of the Carnegie Ridge, a linear bathymetric high on the subducting Nazca Plate in the Eastern Pacific, has strongly impacted magmatism and tectonic activity in the Ecuadorian Andes. We employed radioisotopic dating techniques and numerical modeling to evaluate the uplift of Andes by exploiting information contained in certain minerals that record the cooling of rock as mountain ranges are uplifted, and eroded. The cooling histories of rocks from the Western Cordillera in Ecuador reveal two distinct phases of cooling. The first phase of cooling occurred shortly after magmatic bodies were emplaced in the Western Cordillera. The second phase began after 6 Ma, which we attribute to the onset of uplift and erosion in the Western Cordillera, coeval with the last cooling phase in the Eastern Cordillera. Based on these findings we suggest that the onset of subduction of the Carnegie Ridge increased the coupling between the two plates and promoted shortening and regional rock uplift in this part of the Andes.

1 Introduction

The topography and morphology of the Andes results from crustal shortening and thickening associated with the convergence of the oceanic Nazca Plate and the continental South American Plate as well as superposed climate-driven surface processes. At the orogen-scale, slab geometry, inherited heterogeneities, and lithospheric strength exert first-order controls on deformation, uplift, and magmatic processes, and thus topography of the upper plate (e.g., Isacks, 1988; Horton and Fuentes, 2016; Rodriguez Picada et al., 2022). At a more regional scale, the presence of bathymetric highs on the downgoing Nazca Plate also influences the tectono-magmatic and topographic evolution the overriding plate (e.g., Barberi et al., 1988; Espurt et al., 2007; Wipf et al., 2008; Georgieva et al., 2016). Several field studies relate Quaternary coastal uplift, documented by uplifted marine terraces, to the subduction of bathymetric highs such as sea mounts or aseismic ridges (e.g., Macharé and Ortlieb, 1992; Gardner et al., 1992; Hsu, 1992; Pedoja et al., 2006; Saillard et al., 2011; Freisleben et al., 2021). On larger spatial scales, long-wavelength uplift of the Amazonian foreland is thought to reflect basal shear and thickening of the lower crust associated with the subduction of the Nazca Ridge underneath the Central Andes (e.g., Espurt et al., 2010; Bishop et al., 2018). Modeling studies suggest that subduction of bathymetric highs enhances upper-plate deformation and promotes regional uplift that propagates away from the trench when the subduction of a ridge initiates (e.g., Dominguez et al., 2000; Gerya et al., 2009; Martinod et al., 2013). While the influence of aseismic ridge subduction in the topographically low forearc and foreland regions is reasonably well documented, the influence of ridge subduction on the high-elevation regions of the northern Andes has remained uncertain. Some authors suggest that the subduction of the Nazca Ridge and subsequent slab flattening triggered regional uplift in the Western Cordillera and the Subandes of northern Peru (e.g., Margirier et al., 2015; Bishop et al., 2018), but the relative importance of ridge subduction versus the change in slab geometry is unknown. Other studies relate uplift and exhumation of the East-

ern Cordillera in Ecuador and Colombia to ridge subduction (Spikings et al., 2001, 2010; Spikings and Simpson, 2014); however, owing to shortening phases unrelated to ridge subduction in the eastern side of the Andes (e.g., Mégar, 1984; Sébrier et al., 1988), the link between exhumation in this area and ridge subduction is not straightforward.

The oblique subduction of the aseismic Carnegie Ridge in Ecuador (Fig. 1) has strongly impacted the geological evolution of the northern Andes by promoting strike-slip faulting and the northward motion of the North Andean Sliver, reactivating inherited tectonic structures (e.g., Egbue and Kellog, 2010; Schütt and Whipp, 2020), and driving changes in magmatism (e.g., Barberi et al., 1988; Bourdon et al., 2003; Chiaradia et al., 2020). Despite its importance for the evolution of the northern Andes, neither the timing of ridge subduction nor its potential impact on uplift and exhumation are well constrained. To unravel these relationships, we present new geochronological and thermochronological data from the previously sparsely dated Western Cordillera integrated with structural information (e.g., Daly, 1989; Eguez et al., 2003), geochemistry (e.g., Bourdon et al., 2003; George et al., 2020), and existing thermochronological data (Spikings et al., 2000, 2001, 2004, 2010; Winkler et al., 2005) to decipher the effect of the onset of ridge subduction, its timing, and the spatiotemporal patterns of exhumation above the subducted portions of the Carnegie Ridge.

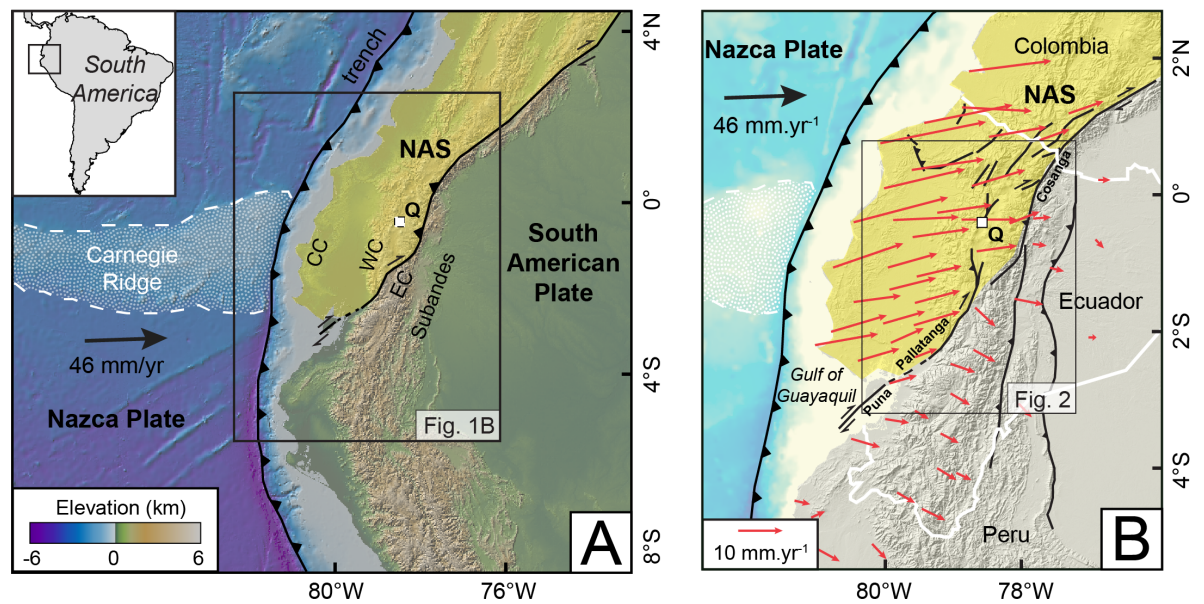


Figure 1. a) Geodynamic setting and topography of the Ecuadorian Andes with bathymetry and Carnegie Ridge. The North Andean Sliver (NAS) is highlighted in yellow. The inset shows the location of study area. b) Active faults (Alvarado et al., 2016; black lines)

and GPS horizontal velocity field (red arrows) with respect to stable South America (Nocquet et al., 2014).

2 Geologic and geodynamic setting

2.1 Cenozoic tectonics and exhumation history of the Ecuadorian Andes

The Ecuadorian Andes constitute a bivergent orogen with active thrusting at the western flank of the Western Cordillera (Eguez et al., 2003; Jaillard et al., 2004; Jaillard et al., 2005) and in the Subandes in the east (Baby et al., 2013). Currently, transpression dominates this region, which causes the northward extrusion of the North Andean Sliver along the dextral Puna-Pallatanga-Cosanga fault system (e.g., Alvarado et al., 2016).

The Western and Eastern cordilleras are separated by the Interandean Valley (Fig. 2), which is filled with Cenozoic volcanic and sedimentary rocks (e.g., Hungerbühler et al., 2002). The Western Cordillera is characterized by a high-elevation (3500 m), low-relief surface capped by Quaternary volcano-sedimentary deposits and Quaternary volcanoes. The western flank of the Western Cordillera is incised by ~2-km-deep valleys exposing Oligocene and Miocene intrusions (31 to 7 Ma; Schütte et al., 2010) and Cretaceous and Paleogene volcano-sedimentary rocks. None of the existing thermochronological data (e.g., Spikings et al., 2005; Winkler et al., 2005; Fig. 2A) has resolved the most recent exhumation history of the Western Cordillera that was associated with topographic growth and valley incision on its western flank. Thermochronological data from the Western and Eastern cordilleras record cooling phases at ~65-55 and 43-30 Ma that were associated with Cenozoic accretion events and changes in plate kinematics that led to exhumation (e.g., Spikings et al., 2001). Thermochronological data from the Eastern Cordillera also record several exhumation phases from 15 Ma to the present that have been linked to the onset of ridge subduction and the subduction of a bathymetric high along the subducting ridge (Spikings et al., 2000; 2001; 2004; 2010).

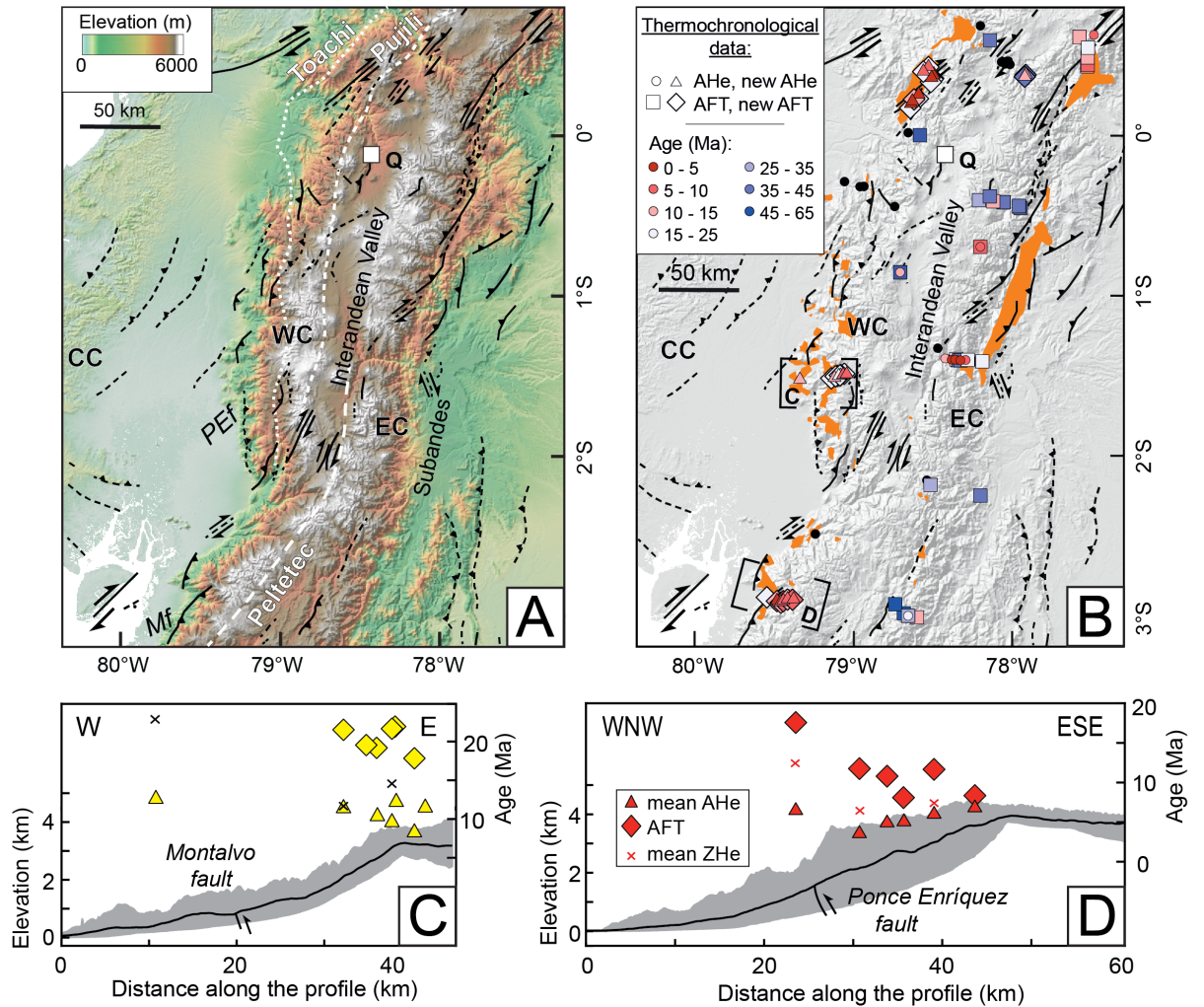


Figure 2. a) Topographic map showing faults (black lines; Eguez et al., 2003), and purported sutures zones (white dashed lines; Alvarado et al., 2014). The Coastal Cordillera (CC), the Western Cordillera (WC) and the Eastern Cordillera (EC) are indicated on the map as well as the Montalvo fault (Mf) and the Ponce Enríquez fault (PEf). b) Existing, and new thermochronological data of the Ecuadorian Andes (non-reset AHe and AFT ages and volcanism ages indicated by black dots; Spikings et al., 2000, 2001, 2004, 2010; Winkler et al., 2005); intrusions (orange) and faults. c, d) Swath profiles across the Montalvo and the Ponce Enríquez reverse faults, respectively and thermochronological ages (Garanda and Cuenca profiles).

2.2 Subduction of the Carnegie Ridge

The aseismic Carnegie Ridge is 200 km wide and rises up to 2 km above the surrounding ocean floor (Fig. 1); it is one of the most prominent bathymetric highs intercepting the South American trench. The oblique subduction of the Carnegie Ridge in Ecuador (Fig. 1) is linked with coastal surface and rock uplift (Pedoja et al., 2006), strike-slip faulting (Fig. 2; e.g., Egbue and Kellogg, 2010; Baize et al., 2015; Alvarado et al., 2016), changes in magmatism, and the extrusion of the North Andean Sliver coeval with the opening of the Gulf of Guayaquil. However, the timing of onset of Carnegie Ridge subduction is controversial. Spikings et al. (2000, 2001, 2004) suggested an early onset of ridge subduction at 15-10 Ma based on the exhumation history of the Eastern Cordillera. Pilger (1984) suggested that the ridge collided at 15 Ma based on a plate-kinematic reconstruction. Using a refined plate-kinematic reconstruction, Daly (1989) suggested a late Miocene (~8 Ma) onset of ridge subduction, which was thought to be in agreement with the timing of arc widening and migration (e.g., Gutscher et al., 1999). Studies based on the timing of submarine canyon incision, marine terrace uplift, and variation in the spatial distribution and chemistry of magmatism have proposed an onset at ~5 Ma (Barberi et al., 1988; Collot et al., 2019; Pedoja et al., 2006; Bourdon et al., 2003). Finally, a Pleistocene onset of ridge subduction was suggested based on plate-kinematic reconstructions (Lonsdale and Klitgord, 1978), a shift toward adakitic arc volcanics at 1.5 Ma (Samaniego et al., 2005), coastal uplift and stratigraphy of marine terraces (Cantalamesa and Di Celma, 2004), and accelerated subsidence and sedimentation rates in the Gulf of Guayaquil. The latter process was associated with accelerated escape of the North Andean Sliver and the geometry of shelf depocenters (e.g., Witt et al., 2006; Hernández et al., 2020).

3 Methods

Low-temperature thermochronology records the thermal history of the crust that can be related to exhumation and/or cooling/heating events. Exhumation can be, with supporting geological information, interpreted as the combined result of rock uplift and erosion. Zircon (U-Th)/He (ZHe), apatite fission track (AFT) and apatite (U-Th)/He (AHe) thermochronometers are sensitive to temperatures ranging from 200 to 20 °C (e.g., Ault et al., 2019). The thermal histories of Cuenca, Guaranda and Apuela regions in the Western Cordillera were determined using QTQt software, which inverts AFT annealing and AHe diffusion parameters for samples with an elevation relationship (Gallagher, 2012). We used zircon U-Pb geochronology conducted at the Arizona LaserChron Center and published data (Schütte et al., 2010) to determine the crystallization ages of intrusions and as a constraint for thermal modeling. Additional methodological details can be found in Supplemental Data (Text S1; Tables S1, S2).

4 Results

4.1 Zircon U-Pb dating

We obtained 5 new zircon U-Pb ages for the intrusions of the Western Cordillera

ranging from 23.9 ± 0.7 to 15.4 ± 0.5 Ma (Fig. 3A; Table 1; Fig. S1). Zircon U-Pb ages from the Apuela Nanegal intrusion in northern Ecuador are 23.9 ± 0.7 (987 m) and 15.4 ± 0.5 Ma (1676 m). In central Ecuador the zircon U-Pb age of the Telimba Chazo Juan intrusion is 21 ± 0.6 Ma (2086 m). In southern Ecuador the zircon U-Pb ages for the Gaby-Papa Grande intrusion and the Chaucha intrusion are 22.7 ± 0.5 Ma (683 m) and 16.9 ± 0.4 Ma (2578 m), respectively.

4.2 Low-temperature thermochronology

We sampled along two structural cross-sections in the central (Guaranda area) and southern parts (Cuenca area) of the Western Cordillera (Fig. 2B, C), spanning an elevation range between 0.9 and 1.4 km. Each transect includes a vertical profile in the hanging wall of the principal reverse fault. We also sampled along a vertical profile in the northern part of the Western Cordillera (Apuela area).

We present 86 AHe single-grain ages for 22 samples, AFT data for 20 samples, and 26 ZHe single-grain ages for 9 samples (Fig. 3; Tables 2, 3, 4; Figs. S2-S7; Tables S3-S24). AHe ages range from 15.4 ± 0.3 to 2.3 ± 0.1 Ma, AFT ages range from 21.7 ± 1.6 to 8.1 ± 1.3 Ma; mean-track lengths are between 13 and 16 μm . For the same samples ZHe ages are younger than AFT ages and range from 23.6 ± 0.3 to 5.9 ± 0.1 Ma (Fig. 3).

Thermochronological ages from the Garanda cross-section are different either side of the Montalvo reverse fault, with mean AHe and ZHe ages being older in the footwall and younger in the hanging wall (Fig. 2B). AFT dates cluster at 20 Ma in the hanging wall and no AFT date is available in the footwall (Fig. 2B). Thermochronological ages from the Cuenca cross-section record a clear pattern with older AHe, AFT and ZHe ages for the samples located in the footwall of the Ponce Enrquez reverse fault and younger ages in the hanging wall (Fig. 2C).

Combined, the samples from the vertical profiles cover an elevation range from 950 to 3100 m (Fig. 3). Early Miocene AFT ages from the Apuela and Garanda areas are similar to the ages of intrusion (Fig. 3A, B). In the Cuenca area AFT ages cluster at ~ 11 Ma, and are largely invariant with elevation (Fig. 3C). AHe ages from the different sampling sites are consistent along the Western Cordillera and show an age-elevation relationship, with a trend toward younger ages at lower elevations (Fig. 3D, E, F). AHe ages from the Cuenca and Apuela area clearly show a positive age-elevation relationship (Fig. 3D, F), with ages ranging from 8.7 ± 0.1 Ma to 2.3 ± 0.1 Ma. AHe ages from the Garanda area show more intersample grain-age dispersion and do not reveal such a clear trend with elevation (Fig. 3E). Here, most samples are located at higher elevation, and AHe ages are dispersed around 12 Ma. ZHe ages increase with elevation at the scale of the Western Cordillera.

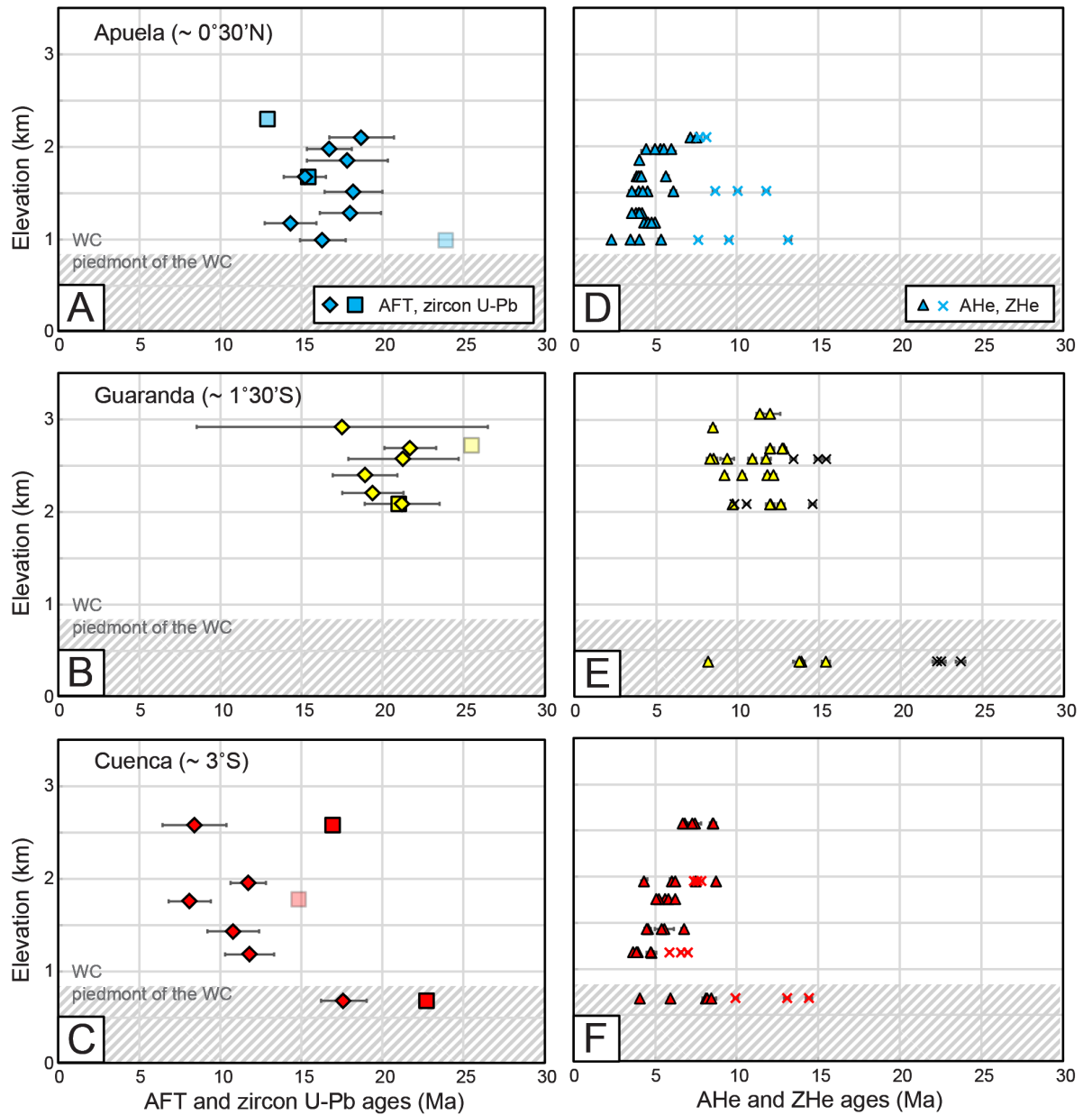


Figure 3. a-c: New AFT ages and zircon U-Pb ages (data from Schütte et al., 2010 are indicated in pastel colors) from the Western Cordillera (WC) plotted against sample elevation for the Apuela, the Guaranda and the Cuenca profiles. d-f: New AHe and ZHe ages from the Western Cordillera plotted against sample elevation for the

Apuela, the Guaranda and the Cuenca profiles.

4.3 Thermal modeling

Thermal histories predicted by QTQt satisfactorily reproduced AHe and AFT data for each profile (Fig. 4). The ZHe thermochronometer has a wide range of temperature sensitivity depending on the radiation damage of the zircons (e.g., Ault et al., 2019). As our ZHe data show no clear correlation between the single-grain ages and eU (Figs. S5-S7), we were not able to reproduce the measured ZHe ages with the diffusion model included in QTQt (i.e., Guenthner et al., 2013); thus the ZHe data were excluded from the thermal modeling.

The thermal histories that best predict the AHe and AFT data from inversion of the three age-elevation profiles indicate rapid cooling immediately after the emplacement of intrusions ($\sim 100^\circ\text{C}/\text{Myr}$); this was followed by residence of the samples at temperatures of $\sim 100^\circ\text{C}$ from 15 to 6 Ma and from 11 to 6 Ma, for the northern and the southern profiles, respectively. The final cooling phase of the overall thermal history initiated between ~ 6 and 5 Ma, and continues to the present-day ($\sim 15^\circ\text{C}/\text{Myr}$). Although the Garanda profile exhibits a similar early cooling history, the older, high-elevation AHe ages cannot resolve the late Miocene cooling history.

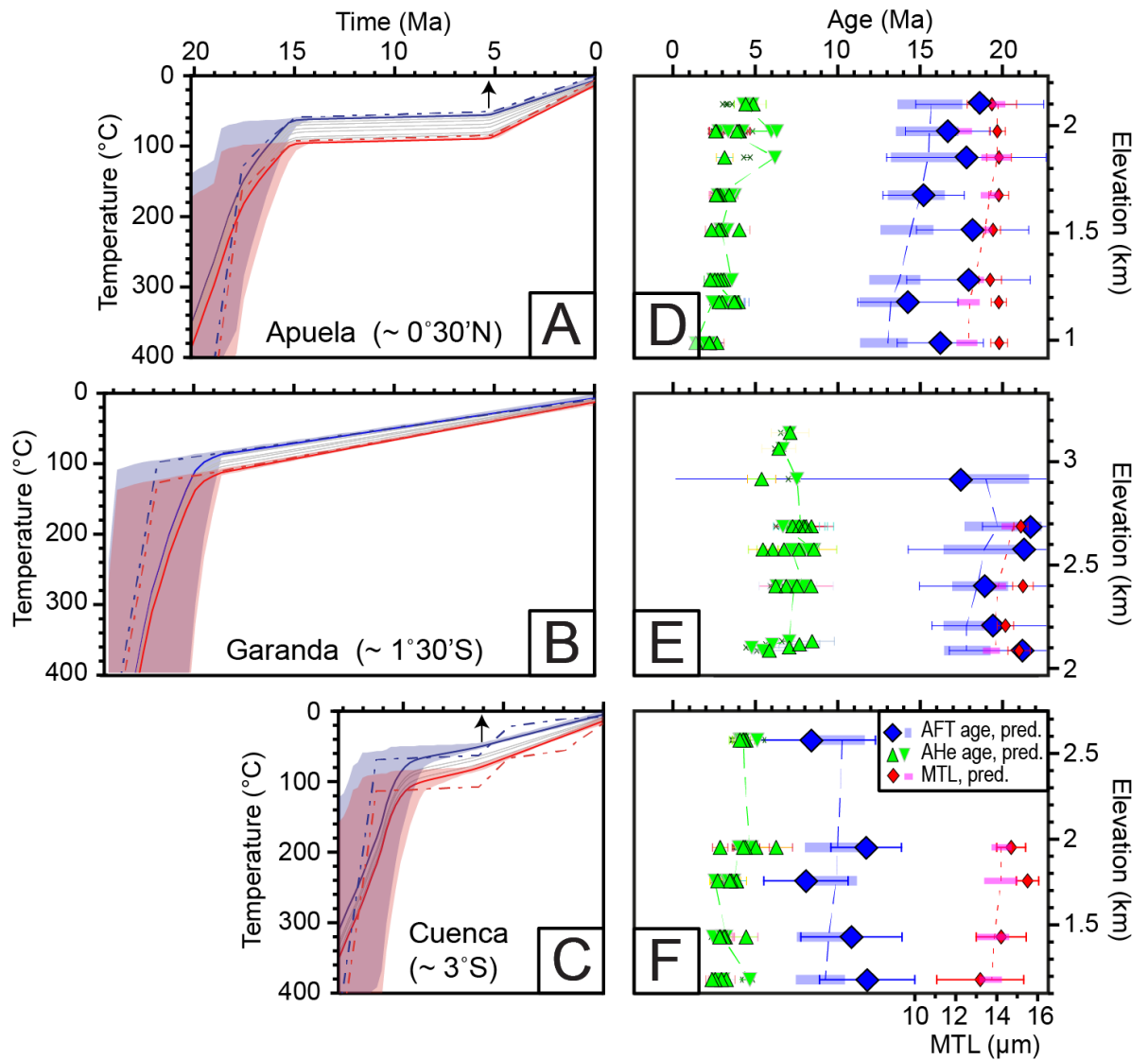


Figure 4. a-c: t-T path for each profile. Each line represents the t-T path of a sample, the red and blue lines represent the t-T path of the lower and upper sample respectively; transparent shading indicates uncertainties. The red and blue dashed lines denote thermal paths that best fit the data. d-f: Age-elevation profiles for the Apuela, Garanda and Cuenca areas showing AFT ages, mean-track length (MTL) and AHe ages; ages predicted based on thermal history are shown by pastel colors.

5. Discussion

5.1 Late Miocene rock uplift and exhumation in the western Ecuadorian Andes

Thermochronological and geochronological data from the Western Cordillera indicate rapid cooling after the early Miocene crystallization of the intrusions (Fig. 4). Initial early Miocene rapid cooling likely corresponds to post-magmatic cooling via thermal relaxation of the intrusions (e.g., Murray et al., 2019), although coeval exhumation cannot be excluded. The most recent cooling histories documented by the Cuenca and the Apuela profiles are consistent and record an isothermal phase followed by a second cooling phase starting at ~6-5 Ma. The isothermal phase suggests that little exhumation occurred in the Western Cordillera between 15 and 6-5 Ma. The second cooling phase in the Western Cordillera is synchronous with the onset of the last cooling phase recorded in the Eastern Cordillera (starting at 5.5 Ma; Spikings and Crowhurst, 2004; Spikings et al., 2010), and with rapid cooling in the Coastal Cordillera between 6 and 5 Ma (Brichau et al., 2021). This late Miocene cooling in both cordilleras is also contemporaneous with the formation of alluvial-fan deposition in the basins to the west and east of the Andes (e.g., Alvarado et al., 2016), supporting the idea that this cooling phase was associated with erosional exhumation. The cooling rate and the geothermal gradient of 30°C/km derived from the modeling of our thermochronological data suggest exhumation rates of ~0.5 km/Myr for the last 6 Myr, with total exhumation of ~3 km achieved since 6 Ma.

In contrast to the simple two-stage cooling history of the Western Cordillera, previous thermochronological studies from the Eastern Cordillera and the Coastal Cordillera have suggested multiple phases of exhumation starting at 15, 9, and 6 Ma, and starting at 6 and 2 Ma, respectively (Spikings et al. 2010; Brichau et al., 2021). AFT data from the Interandean Cuenca Basin suggest that it experienced a cooling history similar to the Eastern Cordillera, including a major cooling event at 9 Ma accompanied by shortening (Steinmann et al., 1999). The AHe ages along the Garanda and Cuenca cross-sections are younger in the hanging wall of the reverse faults, whereas they are older in both the footwall and at high elevations in the hanging wall (Fig. 2B, C). This AHe age pattern suggests uplift of the hanging walls of the Montalvo and Ponce Enrquez reverse faults and internal deformation of the North Andean Sliver. Together with thermal histories obtained for vertical profiles (Fig. 4), the spatial age patterns suggest that shortening along these faults controlled uplift and exhumation in the Western Cordillera during the late Miocene synchronous with shear-zone reactivation in the Western Cordillera (Spikings et al., 2005), and deformation and exhumation along the Eastern Cordillera and the Subandes (Spikings and Crowhurst, 2004; Spikings et al., 2010).

Coltorti et al. (2000) suggested that an extensive low-relief surface in the Western Cordillera at 3500 m was at sea level during the early Pliocene (~5.3 Ma) but became dissected because of uplift in the middle and late Pliocene. In light of our new thermochronological data these observations suggest that cooling in the Western Cordillera involving a total of 3 km of exhumation must have been

associated with rock and surface uplift starting at ~ 6 Ma. In southern Ecuador a low surface elevation in the Western Cordillera prior to 6 Ma is compatible with marine sediments in the inter-Andean basins deposited between 15 and 9 Ma (Steinmann et al., 1999; Hungerbühler et al., 2002). Finally, the combination of sedimentological and thermochronological data from the Western Cordillera and the Eastern Cordillera (i.e., Winkler et al., 2005) suggests limited structural uplift in the Western Cordillera prior to 6 Ma. Thus, the present-day topography of the Ecuadorian Andes, including two parallel, high-elevation mountain ranges separated by an intermontane depression, must have initiated at ~ 6 Ma.

5.2 Implications for the timing of Carnegie Ridge subduction

The subduction of bathymetric highs has been suggested to trigger widespread deformation and uplift in non-collisional orogens (e.g., Lallemand et al., 1992; von Huene et al., 1997; Dominguez et al., 1998; Pubellier et al., 1999; Ramos, 2005; Martinod et al., 2013; Spikings and Simpson, 2014; Georgieva et al., 2016) and island arcs (Taylor et al., 1987; Mann et al., 1998; Rosenbaum and Mo, 2011; Freisleben et al., 2021). In addition, the subduction of oceanic aseismic ridges also appears to cause changes in the geochemical composition of magmatism with a shift to a more juvenile isotope signal (Chiaradia et al., 2020). Our thermochronological data from the Western Cordillera in Ecuador clearly document the onset of a regional uplift and exhumation phase that started at ~ 6 -5 Ma (Fig. 4). Our data suggest that the Ponce Enríquez and Montalvo reverse faults are major structures controlling rock uplift and exhumation in the Western Cordillera. Importantly, these faults appear to be associated with transpression and the extrusion of the North Andean Sliver along the dextral Puna-Pallatanga-Cosanga strike-slip fault. Although the North Andean Sliver may have initiated as early as 15 Ma due to oblique subduction (e.g., Alvarado et al., 2016), the acceleration of northward motion of this block suggests increased coupling at the plate interface after the interception of the Carnegie Ridge (Witt et al., 2006). Importantly, earlier cooling and exhumation phases identified in the Eastern Cordillera and the Coastal Cordillera between 15 and 7 Ma (Spikings et al., 2005, 2010; Bricchau et al., 2021) that have been associated with subduction of the Carnegie Ridge (i.e., Spikings et al., 2010), were synchronous with deformation and uplift recorded at 17-15 Ma, 13 Ma, and 9-8 Ma in the sub-Andes of northern Peru (e.g., Mégard, 1984; Sébrier et al., 1988; Moreno et al., 2020). These earlier cooling phases, however, are not recorded in the Western Cordillera, suggesting that earlier uplift and exhumation in other parts of Ecuador were independent from aseismic ridge subduction processes.

Initial Carnegie Ridge subduction at ~ 6 -5 Ma is consistent with geodynamic reconstructions and with the results of studies of the offshore morphology and subsidence history of the Gulf of Guayaquil that propose an onset of ridge subduction at 5 Ma and document ongoing ridge subduction by ~ 1.8 Ma (e.g., Witt et al., 2006; Collot et al., 2019). Onset of ridge subduction at ~ 6 -5 Ma is also compatible with the timing of regional compressional tectonic inversion of the forearc (Daly, 1989). Moreover, an eastward shift of volcanism at 6-5 Ma

in northern Ecuador (Barberi et al., 1988) and a subsequent change in magma chemistry also support the notion of onset of Carnegie Ridge subduction at this time (e.g., Bourdon et al., 2003; Samadiego et al., 2010).

Taken together, our thermochronological and geochronological data suggest that the subduction of the Carnegie Ridge triggered shortening and exhumation in the Ecuadorian Andes starting at ~6-5 Ma (Fig. 5). However, a delay between the onset of ridge subduction and exhumation processes in the high Andes is possible. Thus, we cannot exclude an onset of Carnegie Ridge subduction at 9-8 Ma as previously suggested by Daly (1989) and Gutscher et al. (1999) based on plate kinematic reconstruction. Finally, Hafnium isotopic compositions of zircons in Ecuador become more juvenile at 8-6 Ma (George et al., 2020) and could also reflect the arrival of the Carnegie Ridge at the trench and ensuing changes in volcanic arc geochemistry at that time.

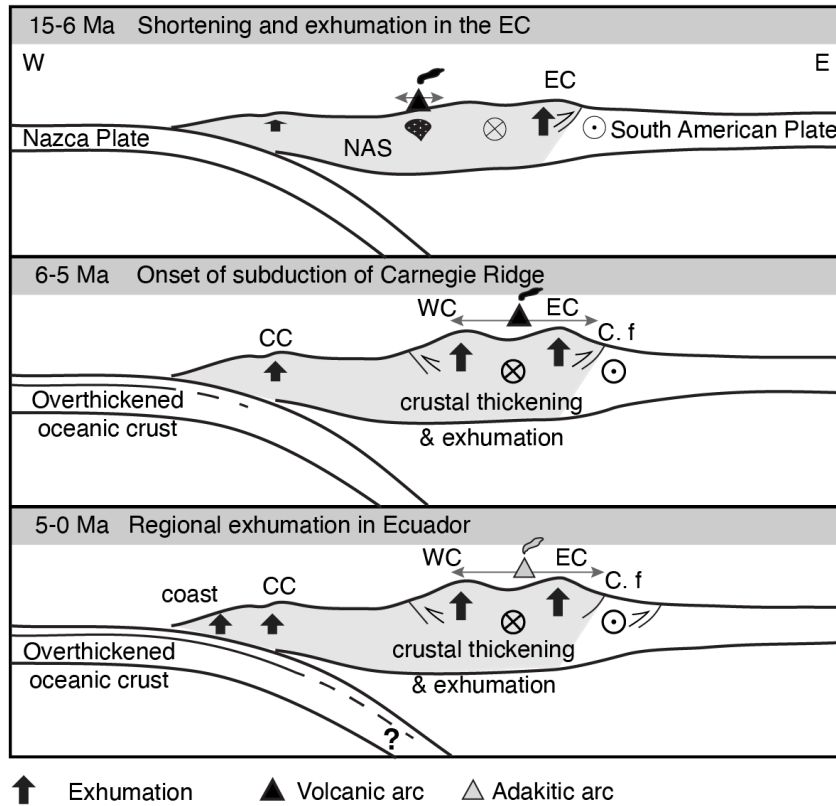


Figure 5: Schematic cross-sections showing tectonic changes and topographic growth in Ecuador (at ~2°S) during the late Cenozoic. The North Andean Sliver (NAS) is indicated in grey. The Coastal Cordillera (CC), Western Cordillera (WC) and the Eastern Cordillera (EC) as well as the position of the magmatic arc (after George et al.,

2021) are showed on the figure.

6. Conclusions

New geochronological and thermochronological data constrain several cooling phases in the Western Cordillera of Ecuador. AFT ages record cooling associated with post-magmatic thermal relaxation of early and middle Miocene intrusions. This suggests that the AFT thermochronometer is not well suited to decipher the exhumation of the Miocene magmatic arc in the northern Andes. Thermal modeling of our data constrains two cooling phases: a post-magmatic cooling during early and middle Miocene associated with thermal relaxation, a period of tectonic quiescence, and a second phase driven by uplift and exhumation since ~6-5 Ma in the Western Cordillera. This latest Miocene onset of exhumation correlates well with the onset of active shortening and rock uplift, as well as coeval exhumation previously identified in the Coastal Cordillera and the Eastern Cordillera of the northern Andes. We propose that the onset of regional shortening and exhumation at ~6-5 Ma was triggered by the effects of initial subduction of the Carnegie Ridge that caused stronger plate coupling.

Acknowledgements

This study was supported by a PRIME grant of the German Academic Exchange Service, funds from the Potsdam University Graduate School, and support for the Arizona LaserChron Center (NSF-EAR 1649254). We thank U. Chowdhury and the students for assistance at the ANGL laboratory.

Open research

The data will be deposited in a trusted repository that supports the FAIR principles by the time our article is accepted, the data is available in the supporting information, tables, and figures for the purposes of peer review.

References cited

- Alvarado, A., Audin, L., Nocquet, J.-M., Jaillard, E., Mothes, P., Jarrin, P., Segovia, M., Rolandone, F., and Cisneros, D., 2016, Partitioning of oblique convergence in the Northern Andes subduction zone: Migration history and the present-day boundary of the North Andean Sliver in Ecuador: *Tectonics*, v. 35, no. 5, p. 1048-1065, doi: 10.1002/(ISSN)1944-9194.
- Ault, A. K., Gautheron, C., & King, G. E., 2019, Innovations in (U-Th)/He, fission track, and trapped charge thermochronometry with applications to earthquakes, weathering, surface-mantle connections, and the growth and decay of mountains. *Tectonics*, v. 38, p. 3705-3739. <https://doi.org/10.1029/2018TC005312>
- Baby, P., Rivadeneira, M., Barragán, R., and Christophoul, F., 2013, Thick-skinned tectonics in the Oriente foreland basin of Ecuador: Geological Society, London, Special Publications, v. 377, no. 1, p. 59-76, doi: 10.1785/gssrl.67.6.27.

- Baize, S., Audin, L., Winter, T., Alvarado, A., Moreno, L.P., Taïpe, M., Reyes, P., Kauffmann, P. and Yepes, H., 2015. Paleoseismology and tectonic geomorphology of the Pallatanga fault (Central Ecuador), a major structure of the South-American crust. *Geomorphology*, v. 237, pp.14-28.
- Barberi, F., Coltelli, M., and Ferrara, G., 1988, Plio-quaternary volcanism in Ecuador: *Geological Magazine*, v. 125, no. 1, p. 1-14.
- Bishop, B.T., Beck, S.L., Zandt, G., Wagner, L.S., Long, M.D., and Tavera, H., 2018, Accepted Manuscript: *Tectonophysics*, v. 731, p. 73-84, doi: 10.1016/j.tecto.2018.03.005.
- Bourdon, E., Eissen, J.-P., Gutscher, M.-A., Monzier, M., Hall, M.L., and Cotten, J., 2003, Magmatic response to early aseismic ridge subduction: the Ecuadorian margin case (South America): *Earth and Planetary Science Letters*, v. 205, no. 3, p. 123–138.
- Brichau, S., Reyes, P., Gautheron, C., Hernández, M., Michaud, F., Leisen, M., Vacherat, A., Saillard, M., Proust, J.N., and O’Sullivan, P., 2021, First timing constraints on the Ecuadorian Coastal Cordillera exhumation: geodynamic implications: *Journal of South American Earth Sciences*, v. 105, 103007, p. 1–57.
- Cantalamessa, G., and Di Celma, C., 2004, Origin and chronology of Pleistocene marine terraces of Isla de la Plata and of flat, gently dipping surfaces of the southern coast of Cabo San Lorenzo (Manabí, Ecuador): *Journal of South American Earth Sciences*, v. 16, no. 8, p. 633-648.
- Chiaradia, M., Müntener, O. and Beate, B., 2020. Effects of aseismic ridge subduction on the geochemistry of frontal arc magmas. *Earth and Planetary Science Letters*, v. 531, 115984.
- Collet, J.-Y., Ratzov, G., Silva, P., Proust, J.N., Migeon, S., Hernández, M.J., Michaud, F., Pazmino, A., Barba Castillo, D., Alvarado, A., and Khurama, S., 2019, The Esmeraldas Canyon: A Helpful Marker of the Pliocene-Pleistocene Tectonic Deformation of the North Ecuador-Southwest Colombia Convergent Margin: *Tectonics*, v. 38, no. 8, p. 3140–3166, doi: 10.1190/1.9781560801580.
- Coltorti, M., and Ollier, C.D., 2000, Geomorphic and tectonic evolution of the Ecuadorian Andes: *Geomorphology*, v. 32, p. 1–19.
- Daly, M.C., 1989, Correlations between Nazca/Farallon Plate kinematics and forearc evolution in Ecuador: *Tectonics*, v. 8, no. 4, p. 769–790.
- Dominguez, S., Lallemand, S.E., Malavieille, J., and von Huene, R., 1998, Upper plate deformation associated with seamount subduction: *Tectonophysics*, v. 293, no. 3-4, p. 207-224.
- Dominguez, S., Malavieille, J. and Lallemand, S.E., 2000. Deformation of accretionary wedges in response to seamount subduction: Insights from sandbox experiments: *Tectonics*, v. 19, no. 1, p. 182-196.

- Donelick, R.A., 1993. Apatite etching characteristics versus chemical composition. *Nuclear Tracks and Radiation Measurements*, 21(604), pp.1359-0189.
- Egbue, O. and Kellogg, J., 2010. Pleistocene to present North Andean “escape”: *Tectonophysics*, v. 489, no. 1-4, p. 248-257.
- Eguez, A., Alvarado, A., Yepes, H., Machette, M.N., Costa, C., Dart, R.L., and Bradley, L.-A., 2003, Database and Map of Quaternary Faults and Folds of Ecuador and its offshore regions: Open-File Report 03-289, U.S. Geological Survey.
- Espurt, N., Baby, P., Brusset, S., Roddaz, M., Hermoza, W., Regard, V., Antoine, P.O., Salas-Gismondi, R., and Bolanos, R., 2007, How does the Nazca Ridge subduction influence the modern Amazonian foreland basin?: *Geology*, v. 35, no. 6, p. 515, doi: 10.1130/G23237A.1.
- Espurt, N., Baby, P., Brusset, S., Roddaz, M., Hermoza, W. and Barbarand, J., 2010. The Nazca Ridge and uplift of the Fitzcarrald Arch: implications for regional geology in northern South America. *Amazonia: Landscape and Species Evolution: A Look into the Past*. Wiley-Blackwell, p. 89-100.
- Evans, N.J., Byrne, J.P., Keegan, J.T. and Dotter, L.E., 2005, Determination of uranium and thorium in zircon, apatite, and fluorite: Application to laser (U-Th)/He thermochronology: *Journal of Analytical Chemistry*, v. 60, no. 12, p.1159-1165.
- Farley, K.A. and Stockli, D.F., 2002, (U-Th)/He dating of phosphates: Apatite, monazite, and xenotime: *Reviews in mineralogy and geochemistry*, v. 48, no. 1, p.559-577.
- Flowers, R.M., Ketcham, R.A., Shuster, D.L. and Farley, K.A., 2009. Apatite (U–Th)/He thermochronometry using a radiation damage accumulation and annealing model. *Geochimica et Cosmochimica acta*, 73(8), pp.2347-2365.
- Freisleben, R., Jara-Muñoz, J., Melnick, D., Martínez, J. M., and Strecker, M. R., 2021, Marine terraces of the last interglacial period along the Pacific coast of South America (1° N–40° S). *Earth System Science Data*, v. 13, no. 6, p. 2487-2513.
- Gallagher, K., 2012, Transdimensional inverse thermal history modeling for quantitative thermochronology: *Journal of Geophysical Research*, v. 117, no. B2, p. B02408.
- Gardner, T.W., Verdonck, D., Pinter, N.M., Slingerland, R., Furlong, K.P., Bullard, T.F. and Wells, S.G., 1992, Quaternary uplift astride the aseismic Cocos ridge, Pacific coast, Costa Rica: *Geological Society of America Bulletin*, v. 104, no. 2, p. 219-232.
- Gautheron, C., Tassan-Got, L., Barbarand, J. and Pagel, M., 2009. Effect of alpha-damage annealing on apatite (U–Th)/He thermochronology. *Chemical Geology*, 266(3-4), pp.157-170.

- Gehrels, G.E., Valencia, V.A. and Ruiz, J., 2008. Enhanced precision, accuracy, efficiency, and spatial resolution of U-Pb ages by laser ablation–multicollector–inductively coupled plasma–mass spectrometry. *Geochemistry, Geophysics, Geosystems*, 9(3).
- Gehrels, G. and Pecha, M., 2014. Detrital zircon U-Pb geochronology and Hf isotope geochemistry of Paleozoic and Triassic passive margin strata of western North America. *Geosphere*, 10(1), pp.49-65.
- George, S.W.M., Horton, B.K., Vallejo, C., Jackson, L.J., Gabriela Gutierrez, E., 2021, Did accretion of the Caribbean oceanic plateau drive rapid crustal thickening in the northern Andes?: *Geology*, v. 49, no. 8, p. 936-940.
- Georgieva, V., Melnick, D., Schildgen, T.F., and Ehlers, T.A., 2016, Tectonic control on rock uplift, exhumation, and topography above an oceanic ridge collision: Southern Patagonian Andes (47°S), Chile: *Tectonics*, v. 35, no. 6, 1317-1341.
- Gerya, T. V., Fossati, D., Cantieni, C., & Seward, D., 2009, Dynamic effects of aseismic ridge subduction: numerical modelling: *European Journal of Mineralogy*, v. 21, no. 3, p. 649-661.
- Ginster, U., Reiners, P.W., Nasdala, L. and Chanmuang, C., 2019. Annealing kinetics of radiation damage in zircon. *Geochimica et Cosmochimica Acta*, 249, pp.225-246.
- Guenther, W.R., Reiners, P.W., Ketcham, R.A., Nasdala, L. and Giester, G., 2013, Helium diffusion in natural zircon: Radiation damage, anisotropy, and the interpretation of zircon (U-Th)/He thermochronology: *American Journal of Science*, v. 313, no. 3, p. 145-198.
- Gutscher, M.A., Malavieille, J., Lallemand, S., and Collot, J.-Y., 1999, Tectonic segmentation of the North Andean margin: impact of the Carnegie Ridge collision: *Earth and Planetary Science Letters*, v. 168, no. 3, p. 255–270.
- Hernández, M. J., Michaud, F., Collot, J. Y., Proust, J. N., & d’Acremont, E., 2020, Evolution of the Ecuador offshore nonaccretionary-type forearc basin and margin segmentation: *Tectonophysics*, v. 781, 228374.
- Horton, B.K., and Fuentes, F., 2016, Sedimentary record of plate coupling and decoupling during growth of the Andes: *Geology*, v. 44, no. 8, p. 647–650.
- Hsu, J.T., 1992, Quaternary uplift of the Peruvian coast related to the subduction of the Nazca Ridge: 13.5 to 15.6 degrees south latitude: *Quaternary International*, v. 15, p. 87-97.
- Hungerbühler, D., M. Steinmann, W. Winkler, D. Seward, A. Egüez, D. E. Peterson, U. Helg, and C. Hammer, 2002, Neogene stratigraphy and Andean geodynamics of southern Ecuador: *Earth-Science Reviews*, v. 57, no. 1-2, p. 75-124.

- Hurford, A.J. and Green, P.F., 1982, A users' guide to fission track dating calibration. *Earth and Planetary Science Letters*, v. 59, no. 2, p.343-354.
- Isacks, B.L., 1988, Uplift of the central Andean plateau and bending of the Bolivian orocline: *Journal of Geophysical Research: Solid Earth* (1978–2012), v. 93, no. B4, p. 3211–3231.
- Jaillard, E., Ordonez, M., Suárez, J., Toro, J., Iza, D., and Lugo, W., 2004, Stratigraphy of the late Cretaceous–Paleogene deposits of the Cordillera Occidental of central Ecuador: geodynamic implications, *Journal of South American Earth Sciences*, v. 17, no. 1, p. 49-58.
- Jaillard, E., Guillier, B., Bonnardot, M.-A., Hassani, R., Lapierre, H., and Toro, J., 2005, Orogenic buildup of the Ecuadorian Andes, *6th International Symposium on Andean Geodynamics (Barcelona)*, extended abstract, p. 404-407.
- Ketcham, R.A., Carter, A., Donelick, R.A., Barbarand, J. and Hurford, A.J., 2007. Improved modeling of fission-track annealing in apatite. *American Mineralogist*, 92(5-6), pp.799-810.
- Ketcham, R.A., Gautheron, C. and Tassan-Got, L., 2011. Accounting for long alpha-particle stopping distances in (U–Th–Sm)/He geochronology: Refinement of the baseline case: *Geochimica et Cosmochimica Acta*, v. 75, no. 24, p.7779-7791.
- Lallemand, S. E., Malavieille, J., and Calassou, S., 1992, Effects of oceanic ridge subduction on accretionary wedges: experimental modeling and marine observations: *Tectonics*, v. 11, no. 6, p. 1301-1313.
- Laslett, G.M., Galbraith, R.F. and Green, P.F., 1994, The analysis of projected fission track lengths: *Radiation measurements*, v. 23, no. 1, p.103-123.
- Lonsdale, P., and Klitgord, K.D., 1978, Structure and tectonic history of the eastern Panama Basin: *Geological Society of America Bulletin*, v. 89, no. 7, p. 981-999.
- Ludwig, K.R., 2008. User's Manual for Isoplot 3.6 4. *Berkeley Geochronology Center Special Publication*, p.78.
- Macharé, J. and Ortlieb, L., 1992, Plio-Quaternary vertical motions and the subduction of the Nazca Ridge, central coast of Peru: *Tectonophysics*, v. 205, no. 1-3, p. 97-108.
- Mann, P., Taylor, F.W., Lagoe, M.B., Quarles, A. and Burr, G., 1998, Accelerating late Quaternary uplift of the New Georgia Island Group (Solomon island arc) in response to subduction of the recently active Woodlark spreading center and Coleman seamount: *Tectonophysics*, v. 295, no. 3-4, p. 259-306.
- Margirier, A., Robert, X., Audin, L., Gautheron, C., Bernet, M., Hall, S., and Simon-Labric, T., 2015, Slab flattening, magmatism, and surface uplift in the Cordillera Occidental (northern Peru): *Geology*, v. 43, no. 11, p. 1031–1034.

- Martinod, J., Guillaume, B., Espurt, N., and Faccenna, C., 2013, Effect of aseismic ridge subduction on slab geometry and overriding plate deformation: Insights from analogue modeling: *Tectonophysics*, v. 588, p. 39-55.
- Mégard, F., 1984, The Andean orogenic period and its major structures in central and northern Peru: *Journal of the Geological Society*, 141(5), 893-900.
- Michaud, F., Witt, C., and Royer, J.-Y., 2009, Influence of the subduction of the Carnegie volcanic ridge on Ecuadorian geology: Reality and fiction: *Geological Society of America Memoirs*, v. 204, no. 0, p. 217–228, doi: 10.1130/2009.1204(10).
- Moreno, F., Garzzone, C.N., George, S.W., Horton, B.K., Williams, L., Jackson, L.J., Carlotto, V., Richter, F. and Bandeian, A., 2020, Coupled Andean growth and foreland basin evolution, Campanian–Cenozoic Bagua Basin, northern Peru: *Tectonics*, v. 39, no. 7, p.e2019TC005967.
- Murray, K.E., Reiners, P.W., Thomson, S.N., Robert, X. and Whipple, K.X., 2019, The thermochronologic record of erosion and magmatism in the Canyonlands region of the Colorado Plateau: *American journal of science*, v. 319, no. 5, p.339–380.
- Pedoja, K., Dumont, J.F., Lamothe, M., Ortlieb, L., Collot, J.-Y., Ghaleb, B., Auclair, M., Alvarez, V., and Labrousse, B., 2006, Plio-Quaternary uplift of the Manta Peninsula and La Plata Island and the subduction of the Carnegie Ridge, central coast of Ecuador: *Journal of South American Earth Sciences*, v. 22, no. 1-2, p. 1–21, doi: 10.1016/j.jsames.2006.08.003.
- Pilger, R.H., 1984, Cenozoic plate kinematics, subduction and magmatism: South American Andes: *Journal of the Geological Society*, v. 141, no. 5, p. 793-802.
- Pubellier, M., Bader, A. G., Rangin, C., Deffontaines, B., and Quebral, R., 1999, Upper plate deformation induced by subduction of a volcanic arc: the Snellius Plateau (Molucca Sea, Indonesia and Mindanao, Philippines): *Tectonophysics*, v. 304, no. 4, p. 345-368.
- Pullen, A., Ibáñez-Mejía, M., Gehrels, G.E., Giesler, D. and Pecha, M., 2018. Optimization of a laser ablation-single collector-inductively coupled plasma-mass spectrometer (Thermo Element 2) for accurate, precise, and efficient zircon U-Th-Pb geochronology. *Geochemistry, Geophysics, Geosystems*, 19(10), pp.3689-3705.
- Ramos, V.A., 2005, Seismic ridge subduction and topography: Foreland deformation in the Patagonian Andes: *Tectonophysics*, v. 399, no. 1-4, p. 73–86, doi: 10.1016/j.tecto.2004.12.016.
- Reiners, P.W., Spell, T.L., Nicolescu, S. and Zanetti, K.A., 2004, Zircon (U-Th)/He thermochronometry: He diffusion and comparisons with ⁴⁰Ar/³⁹Ar dating: *Geochimica et cosmochimica acta*, v. 68, no. 8, p.1857-1887.

Rodriguez Picada, C., Scheck-Wenderoth, M., Cacace, M., Bott, J., & Strecker, M. R. (2022). Long-term lithospheric strength and upper-plate seismicity in the southern Central Andes, 29°–39°S. *Geochemistry, Geophysics, Geosystems*, v. 23, e2021GC010171.

Rosenbaum, G. and Mo, W., 2011. Tectonic and magmatic responses to the subduction of high bathymetric relief. *Gondwana Research*, v. 19, no. 3, p. 571-582.

Saillard, M., Hall, S.R., Audin, L., Farber, D.L., Regard, V. and Hérail, G., 2011, Andean coastal uplift and active tectonics in southern Peru: 10Be surface exposure dating of differentially uplifted marine terrace sequences (San Juan de Marcona, ~15.4 °S): *Geomorphology*, v. 128, no. 3-4, p. 178-190.

Samaniego, P., Martin, H., Monzier, M., Robin, C., Fornari, M., Eissen, J. P., & Cotten, J., 2005, Temporal evolution of magmatism in the Northern Volcanic Zone of the Andes: the geology and petrology of Cayambe Volcanic Complex (Ecuador): *Journal of petrology*, v. 46, no. 11, p. 2225-2252.

Schütt, J.M., and Whipp, D.M., 2020, Controls on Continental Strain Partitioning Above an Oblique Subduction Zone, Northern Andes: *Tectonics*, v. 39, no. 4, p. 725, doi: 10.1002/2015TC003941.

Schütte, P., Chiaradia, M., and Beate, B., 2010, Geodynamic controls on Tertiary arc magmatism in Ecuador: Constraints from U–Pb zircon geochronology of Oligocene–Miocene intrusions and regional age distribution trends: *Tectonophysics*, v. 489, no. 1-4, p. 159–176, doi: 10.1016/j.tecto.2010.04.015.

Sébrier, M., Mercier, J.L., Macharé, J., Bonnot, D., Cabrera, J., and Blanc, J.L., 1988, The state of stress in an overriding plate situated above a flat slab: The Andes of central Peru: *Tectonics*, v. 7, no. 4, p. 895-928.

Spikings, R.A., and Crowhurst, P.V., 2004, (U-Th)/He thermochronometric constraints on the late Miocene-Pliocene tectonic development of the northern Cordillera Real and the Interandean Depression, Ecuador: *Journal of South American Earth Sciences*, v. 17, no. 4, p. 239–251.

Spikings, R., and Simpson, G., 2014, Rock uplift and exhumation of continental margins by the collision, accretion, and subduction of buoyant and topographically prominent oceanic crust: *Tectonics*, v. 33, no. 5, p. 635-655.

Spikings, R.A., Crowhurst, P.V., Winkler, W., and Villagomez, D., 2010, Syn- and post-accretionary cooling history of the Ecuadorian Andes constrained by their in-situ and detrital thermochronometric record: *Journal of South American Earth Sciences*, v. 30, no. 3-4, p. 121–133, doi: 10.1016/j.jsames.2010.04.002.

Spikings, R.A., Seward, D., Winkler, W., and Ruiz, G.M., 2000, Low-temperature thermochronology of the northern Cordillera Real, Ecuador: Tectonic insights from zircon and apatite fission track analysis: *Tectonics*, v. 19, no. 4, p. 649-668.

Spikings, R.A., Winkler, W., Seward, D., and Handler, R., 2001, Along-strike variations in the thermal and tectonic response of the continental Ecuadorian Andes to the collision with heterogeneous oceanic crust: *Earth and Planetary Science Letters*, v. 186, no. 1, p. 57–73.

Stacey, J.S. and Kramers, J.D., 1975. Approximation of terrestrial lead isotope evolution by a two-stage model: *Earth Planetary Science Letters*, v. 26. *doi*, 10, pp.90088-6.

Steinmann, M., Hungerbühler, D., Seward, D., and Winkler, W., 1999, Neogene tectonic evolution and exhumation of the southern Ecuadorian Andes: a combined stratigraphy and fission-track approach: *Tectonophysics*, v. 307, p. 255–276.

Taylor, F.W., Frohlich, C., Lecolle, J., Strecker, M., 1987, Analysis of partially emerged corals and reef terraces in the central Vanuatu Arc: Comparison of contemporary coseismic and nonseismic with quaternary vertical movements: *Journal of Geophysical Research*, v. 92, no. B6, p. 4905. *doi*:10.1029/JB092iB06p04905.

Von Huene, R., Corvalán, J., Flueh, E. R., Hinz, K., Korstgard, J., Ranero, C. R., and Weinrebe, W., 1997, Tectonic control of the subducting Juan Fernández Ridge on the Andean margin near Valparaiso, Chile: *Tectonics*, v. 16, no. 3, p. 474-488.

Winkler, W., Villagomez, D., Spikings, R., Abegglen, P., Tobler, S., and Eguez, A., 2005, The Chota basin and its significance for the inception and tectonic setting of the inter-Andean depression in Ecuador: *Journal of South American Earth Sciences*, v. 19, no. 1, p. 5–19, *doi*: 10.1016/j.jsames.2004.06.006.

Wipf, M., Zeilinger, G., Seward, D. and Schlunegger, F., 2008. Focused subaerial erosion during ridge subduction: Impact on the geomorphology in south-central Peru. *Terra Nova*, v. 20, no. 1, p.1-10.

Witt, C., Bourgois, J., Michaud, F., Ordoñez, M., Jiménez, N., and Sosson, M., 2006, Development of the Gulf of Guayaquil (Ecuador) during the Quaternary as an effect of the North Andean block tectonic escape: *Tectonics*, v. 25, no. 3, p. TC3017.

Table 1. Zircon U-Pb from the Western Cordillera (Ecuador).

Table 2. Apatite (U-Th-Sm)/He data from the Western Cordillera (Ecuador).

Table 3. Zircon (U-Th)/He single-grain ages from the Western Cordillera (Ecuador).

Table 4. Apatite fission track data from the Western Cordillera (Ecuador).

Tectonics

Supporting Information for

Exhumation of the Western Cordillera, Ecuador driven by late Miocene subduction of the Carnegie Ridge

Audrey Margirier¹, Manfred R. Strecker¹, Peter W. Reiners², Stuart Thomson², Ismael Casado¹, Sarah W.M. George², Alexandra Alvarado³

¹ *Institut für Geowissenschaften, Universität Potsdam, Potsdam, Germany*

² *Department of Geosciences, University of Arizona, Tucson, United States of America*

³ *Instituto Geofísico, Escuela Politécnica Nacional, Quito, Ecuador*

Contents of this file

Text S1-S3
Figures S1 to S7
Captions for Tables S1 to S24

Additional Supporting Information (Files uploaded separately)

Captions for Tables S1 to S24 (if larger than 1 page, upload as separate file)

Introduction

Text S1: Methods

Text S2: Results

Figure S1: AHe age – eU plot for the Cuenca area.

Figure S2: AHe age – eU plot for the Guaranda area.

Figure S3: AHe age – eU plot for the Apuela area.

Figure S4: ZHe age – eU plot for the Cuenca area.

Figure S5: ZHe age – eU plot for the Guaranda area.

Figure S6: ZHe age – eU plot for the Apuela area.

Table S1: Zircon U-Pb ages

Table S2: AFT lengths

Text S1.

Methods

Sampling and mineral separation

Samples were collected in the Western Cordillera in Ecuador (Fig. 2A, Table 1, 2, 3 and 4). Apatite grains were separated by ZirChron (Tucson, USA) using heavy-liquid separation technique (methylene iodide with densities of 2.9 and 3.3).

Zircon U-Pb

Zircon U-Pb geochronology was conducted on a Photon Machines G2 excimer laser coupled to the Element2 mass spectrometer at the Arizona LaserChron Center following in-house procedures. The zircon U-Pb geochronology results are presented in Table 1 and Figure S1. Please refer to Tables 1, S1 and S2 for details of the analytical setting .

Apatite (U-Th-Sm)/He

Apatite (U-Th-Sm)/He analysis were done at the Arizona Noble Gas Laboratory (University of Arizona). Apatite grains were selected according to their morphology, size and purity (absence of visible inclusions; from 1 to 5 grains dated per sample, depending on sample apatite quality). The selected crystals were measured and placed in niobium tubes for He extraction. A diode laser was used to heat the niobium tubes at $1065 \pm 50^\circ\text{C}$ during 3 min to allow a total degassing of radiogenic ^4He . The ^4He content was determined by comparison with a known amount of ^3He spike added during analysis. After He extraction, niobium tubes were placed into single-use polypropylene vials and apatite grains were dissolved for 1 h at 90°C in a $50 \mu\text{l}$ HNO_3 solution containing a known concentration of ^{235}U , ^{230}Th and ^{149}Sm that then was filled with 1 ml of ultrapure MQ water. U, Th-Sm measurements followed a procedure similar to that of Evans et al. (2005). U, Th and Sm concentrations were measured in the solution using an inductively coupled quadrupole plasma mass spectrometry (Element 2 ICP-MS). The analysis was calibrated using external age standards, including Limberg Tuff and Durango apatite. Single ages were corrected using the calculated ejection factor FT, determined using the Monte Carlo simulation technique of Farley and Stockli (2002). The apatite (U-Th-Sm)/He results are presented in Table 2.

Zircon (U-Th-Sm)/He

Zircon (U-Th)/He analysis were performed at the Arizona Noble Gas Laboratory (University of Arizona) following the method described by Reiners et al. (2004). Zircon grains were selected (from 2 to 3 grains dated per sample) according to their morphology, size and the absence of big inclusions. The selected crystals were measured and placed in niobium tubes for He extraction. We used a diode laser to heat the platinum tubes at $1300\pm 100^{\circ}\text{C}$ during 20 min to allow a total He degassing, a reheat under the same conditions allowed checking for the presence of remaining He. The ^4He content was determined by comparison with a known amount of ^3He spike added during analysis. After He extraction zircons were retrieved from the niobium packet and placed into teflon microvials. The samples were spiked with a solution containing a known concentration of ^{233}U , ^{229}Th and dissolved with HF and HNO_3 in Parr bombs. U and Th were measured in a solution using an inductively coupled quadrupole plasma mass spectrometry (Element 2 ICP-MS) at the University of Arizona. The analysis was calibrated using external age standards, including Fish Canyon Tuff zircons. Single ages were corrected using the calculated ejection factor FT, determined using the Monte Carlo simulation technique of Ketcham et al. (2011). The results are presented in Table 3.

AFT analysis

AFT analysis was performed by Stuart Thomson at the University of Arizona. Apatite grains were mounted in epoxy and their surfaces were polished. The mounts were etched with 5.5M HNO_3 for 20 seconds at $20 \pm 1^{\circ}\text{C}$ to reveal spontaneous tracks. AFT ages were obtained with the external detector method (Hurford and Green, 1982) using a zeta calibration approach, with a zeta of 343.1 ± 8.7 for the IRMM 540R dosimeter glass. After etching, muscovite foils, as external detectors, were attached to apatite mounts. Thermal neutron irradiation of the samples was carried out at the Oregon State University Radiation Center with a requested total thermal neutron fluence of 1.2×10^{16} neutrons. cm^2 . After irradiation, mica detectors were etched for 18 minutes in 48% HF at $20 \pm 1^{\circ}\text{C}$ to reveal induced tracks. Tracks were counted and track lengths were measured using an Olympus optical microscope at a magnification of $\times 1250$, according to the recommendations of Laslett *et al.* (1994). AFT ages are reported as central age at $\pm 1\sigma$. Dpar (mean fission-track etch pit diameter, parallel to the C axis of the crystal) measurement was used to estimate the kinetic behavior of single grains (Donelick, 1993). The AFT results are presented in Table 4, the detail of length measurements for each sample is provided in the supplemental tables S3-S24".

Text S2.

Results

Zircon U-Pb

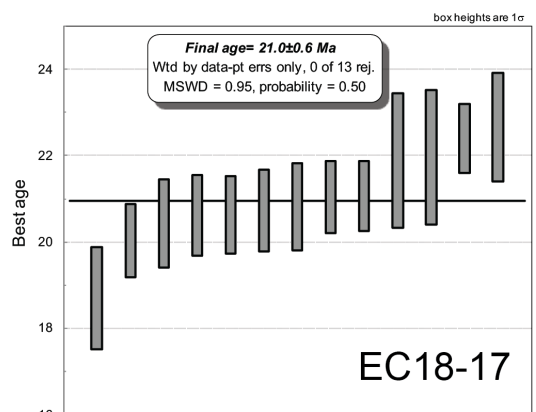
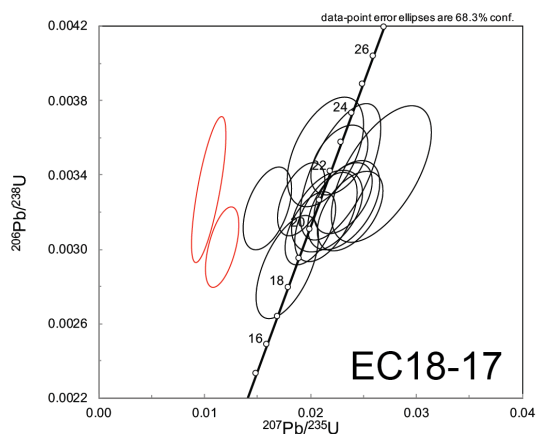
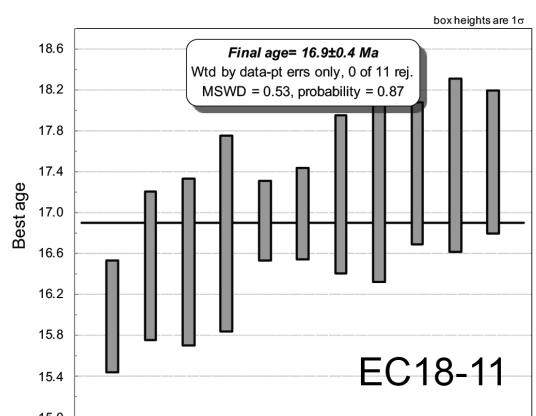
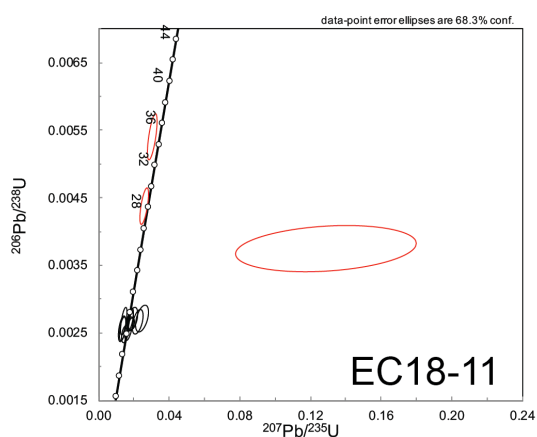
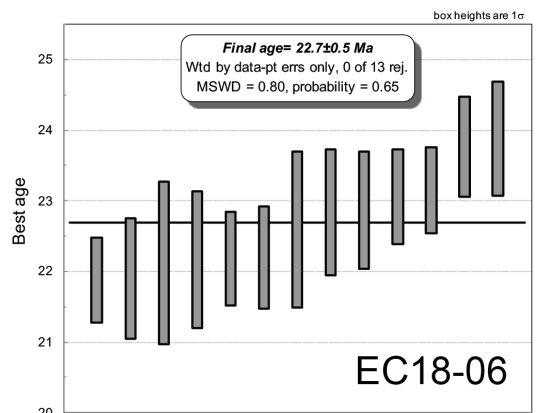
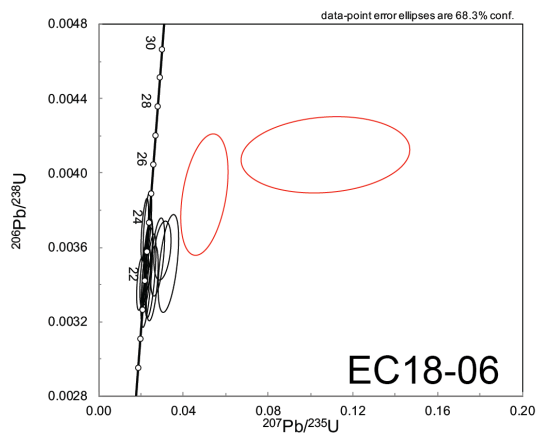


Figure S1. Zircon U-Pb analyses results for samples from the Western Cordillera.

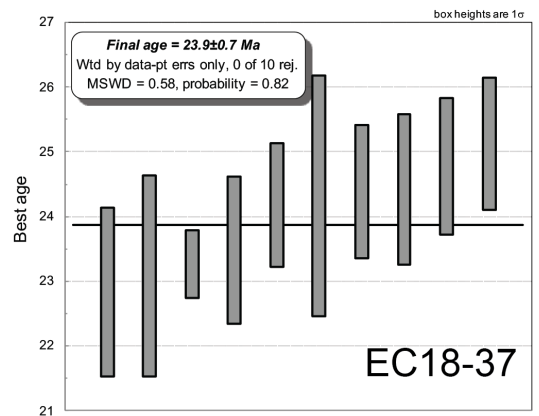
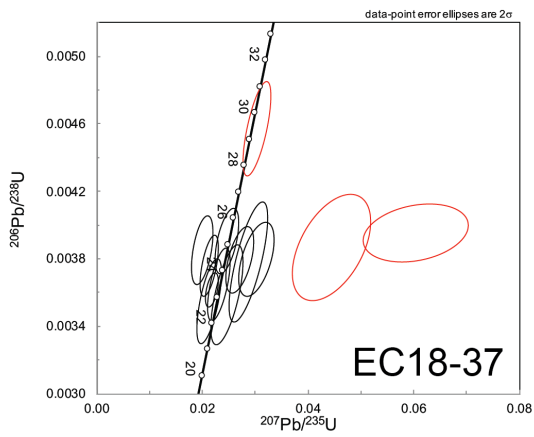
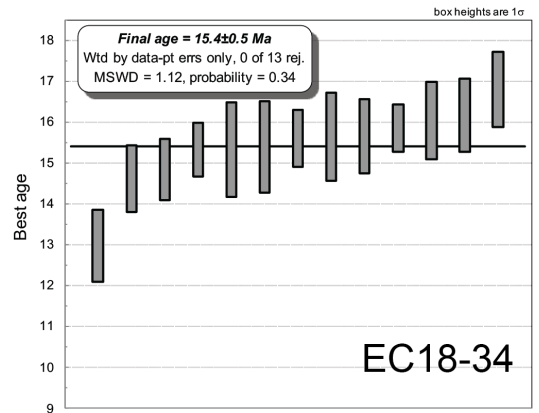
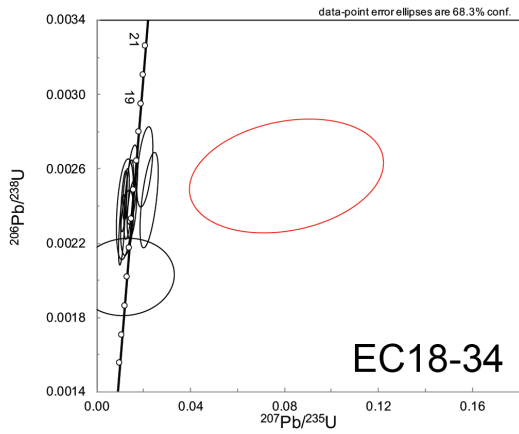


Figure S1 (continued). Zircon U-Pb analyses results for samples from the Western Cordillera.

Apatite (U-Th-Sm)/He

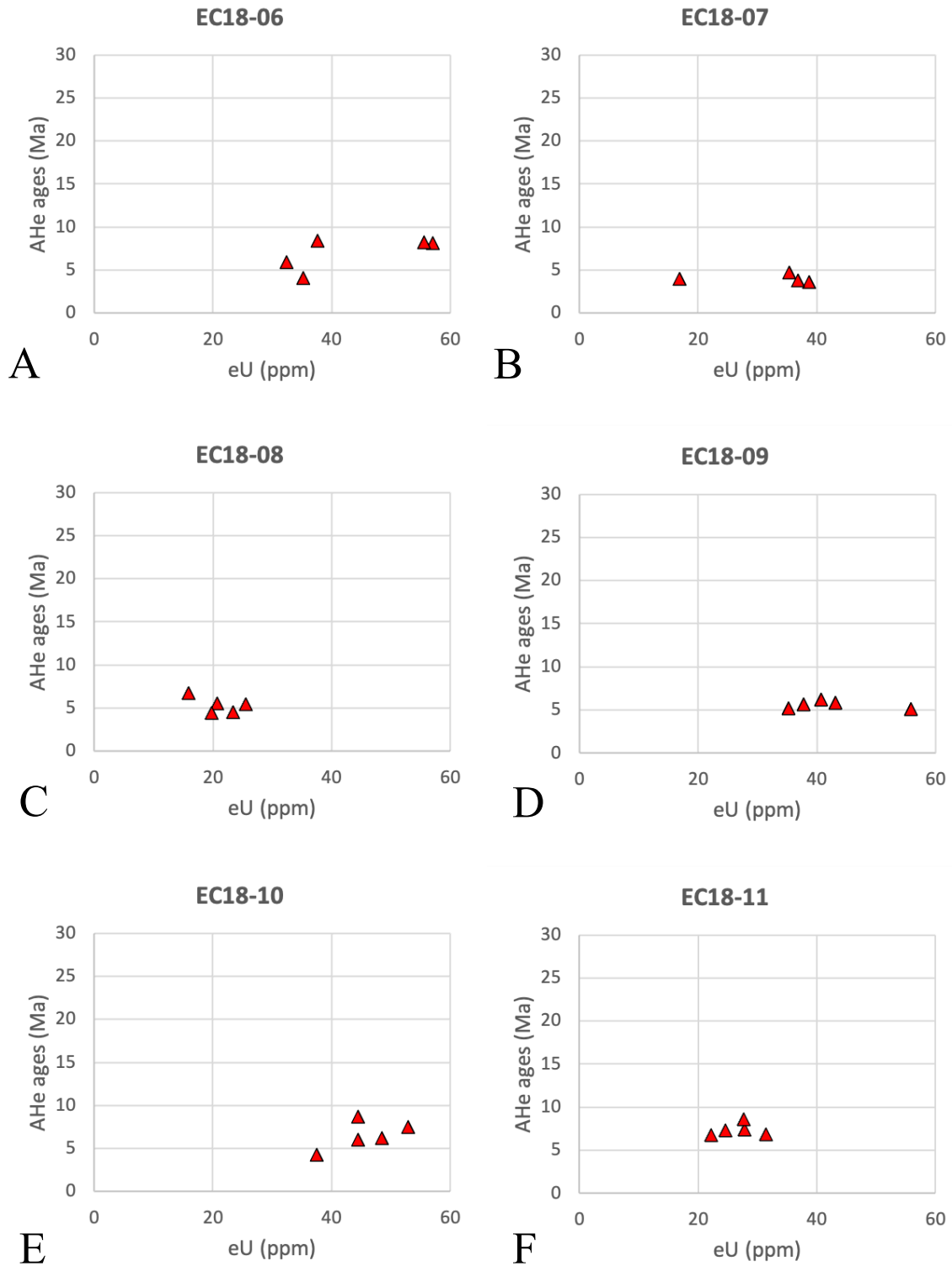


Figure S2. AHe ages – eU plots for samples from the Cuenca area.

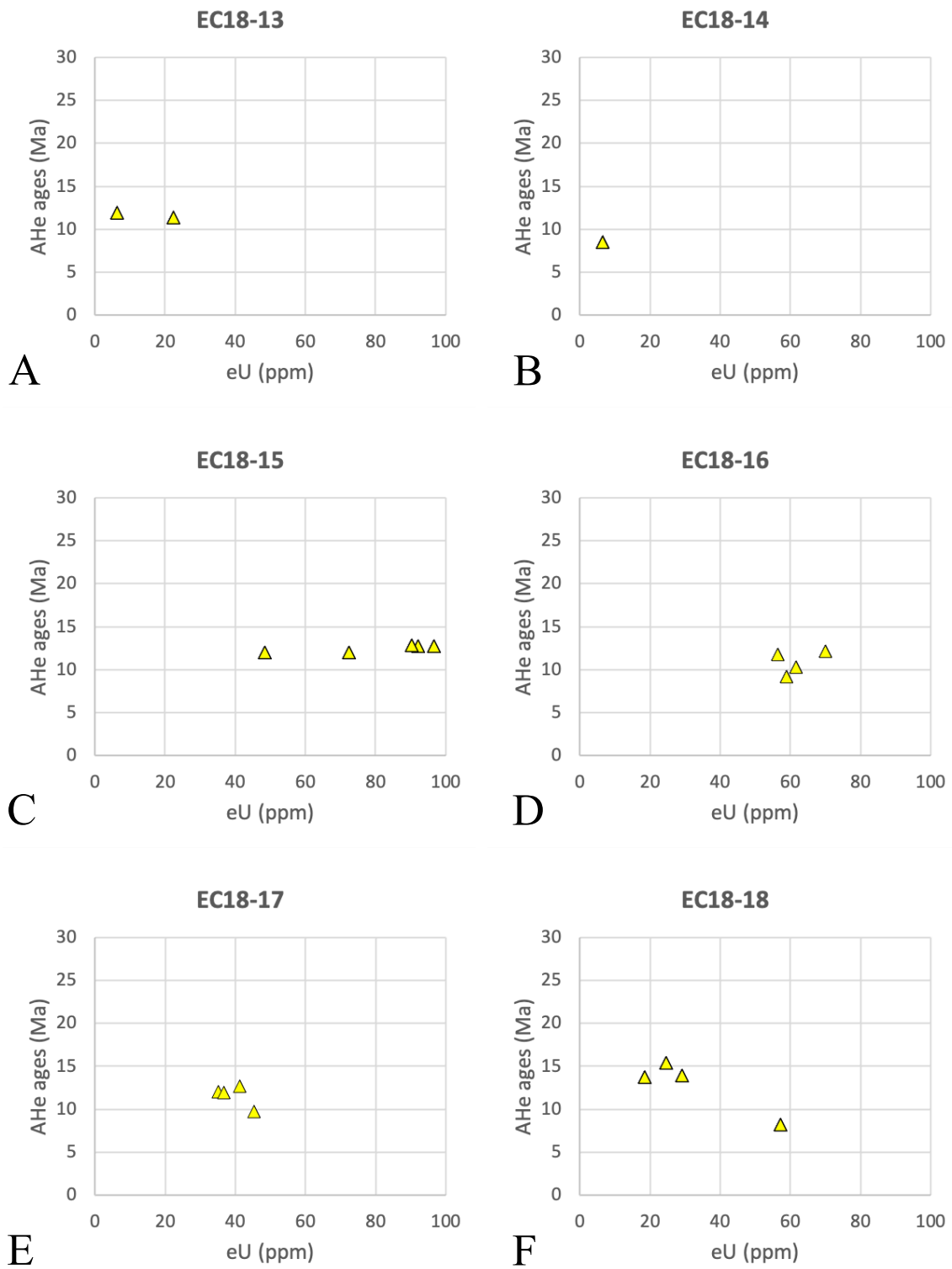


Figure S3. AHe ages – eU plots for samples from the Guaranda area.

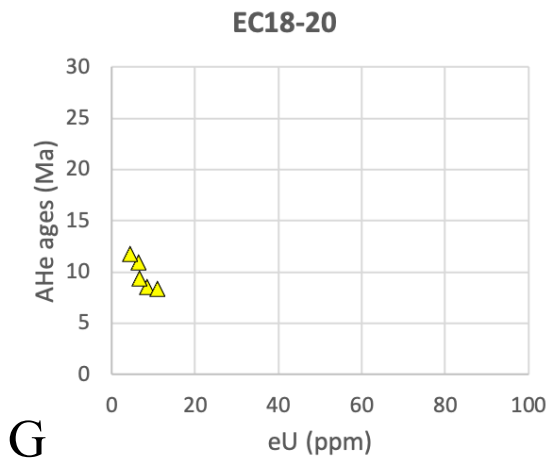


Figure S3 (continued). AHe ages – eU plots for samples from the Guaranda area.

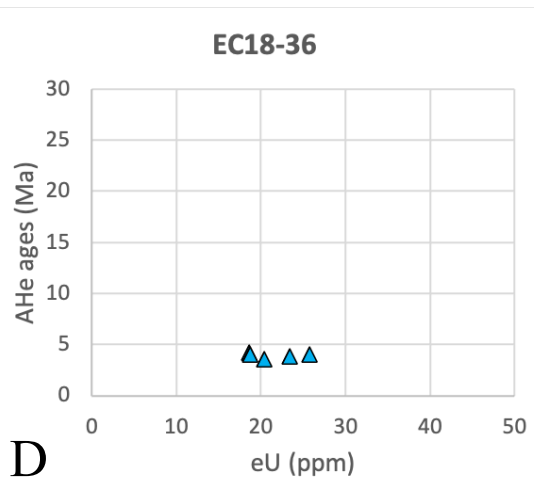
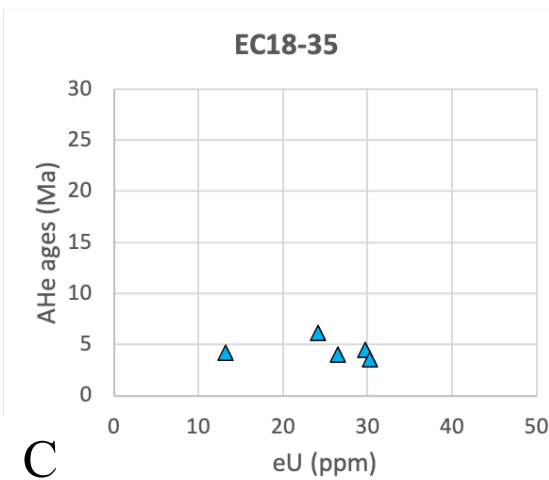
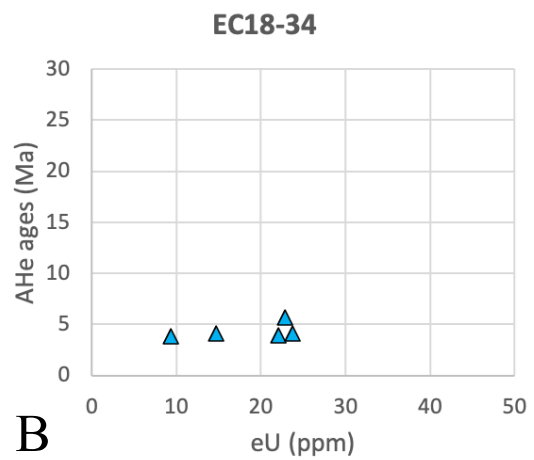
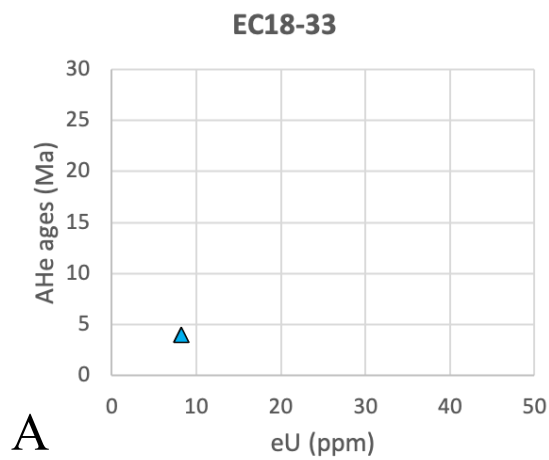


Figure S4. AHe ages – eU plots for samples from the Apuela area.

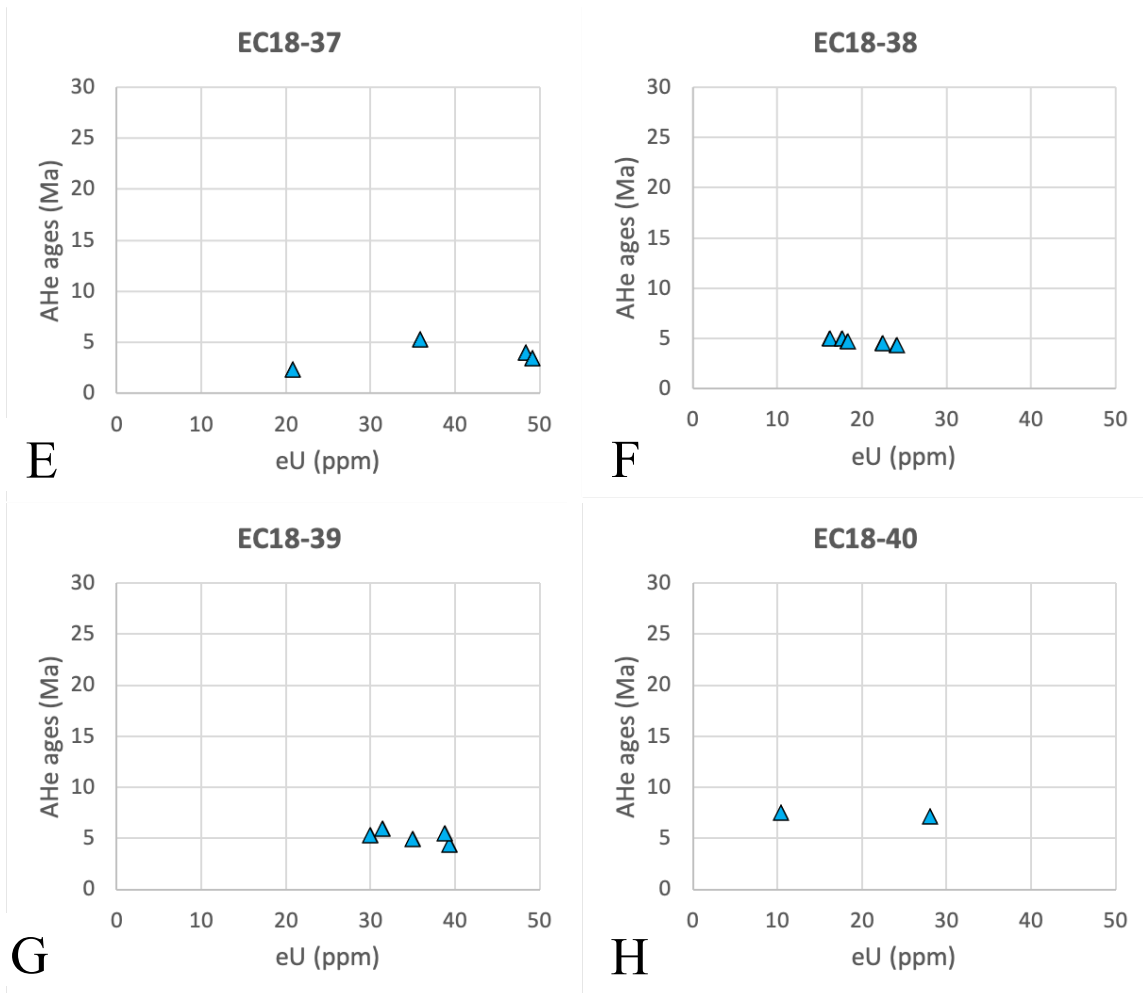


Figure S4 (continued). AHe ages – eU plots for samples from the Apuela area.

Zircon (U-Th)/He

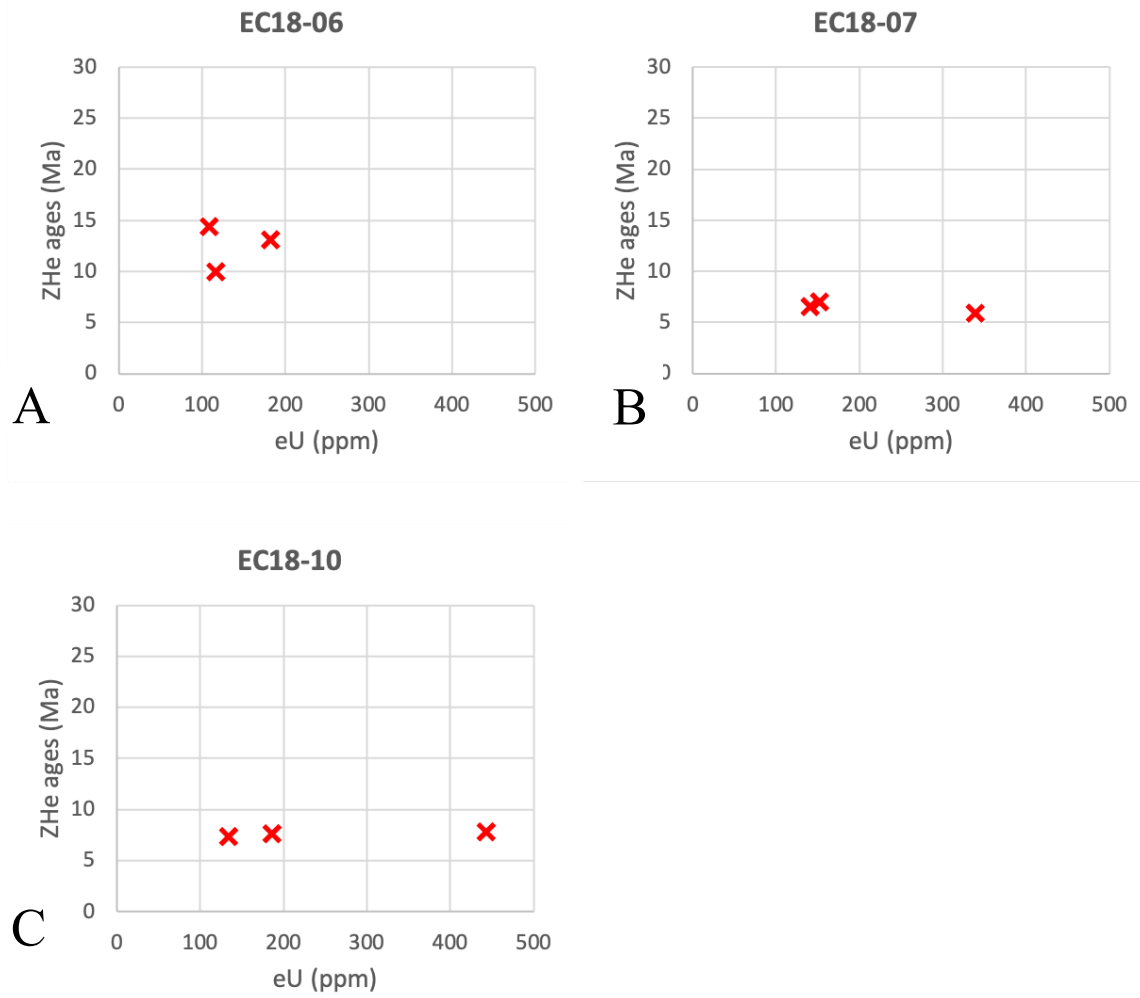


Figure S5. ZHe ages – eU plots for samples from the Cuenca area.

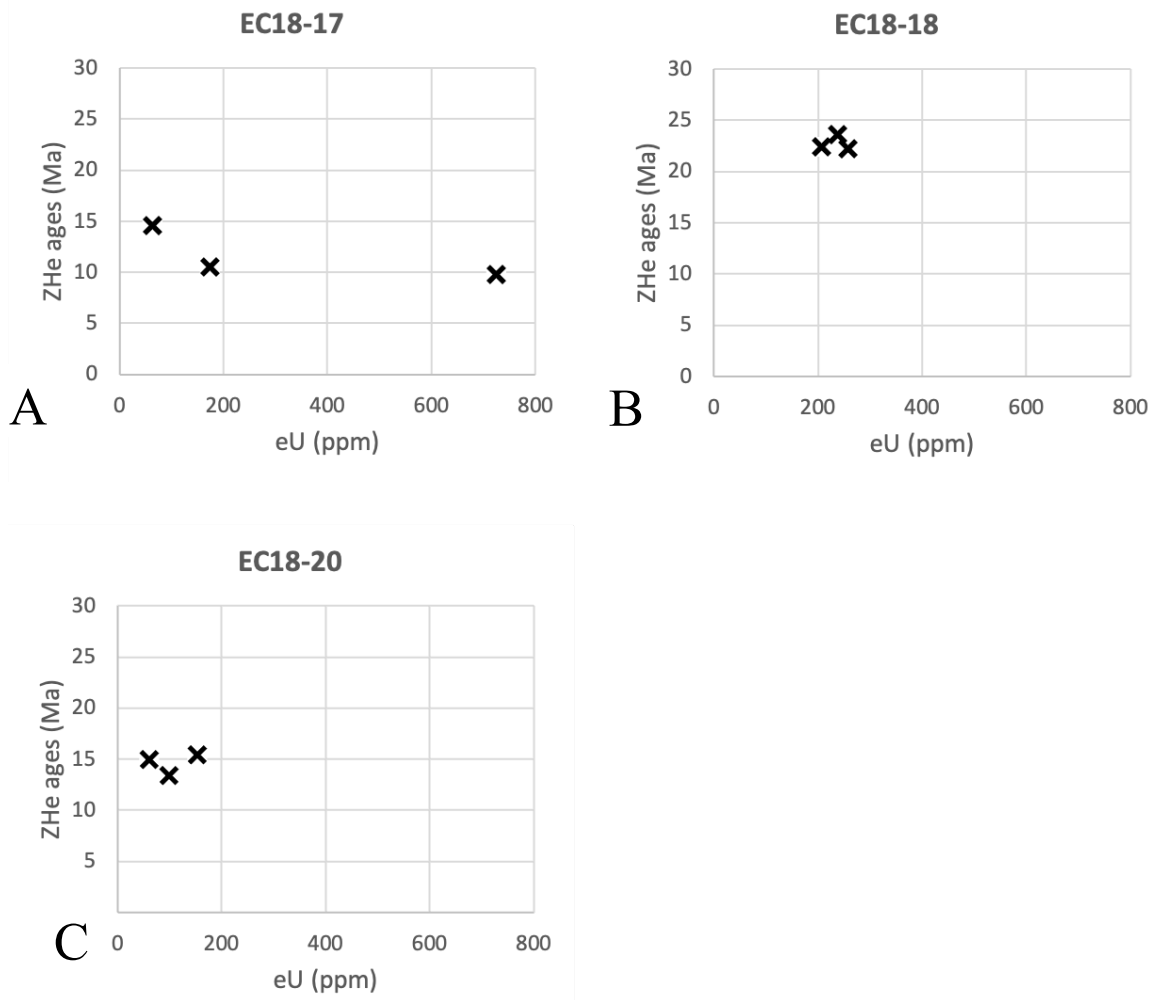


Figure S6. ZHe ages – eU plots for samples from the Guaranda area.

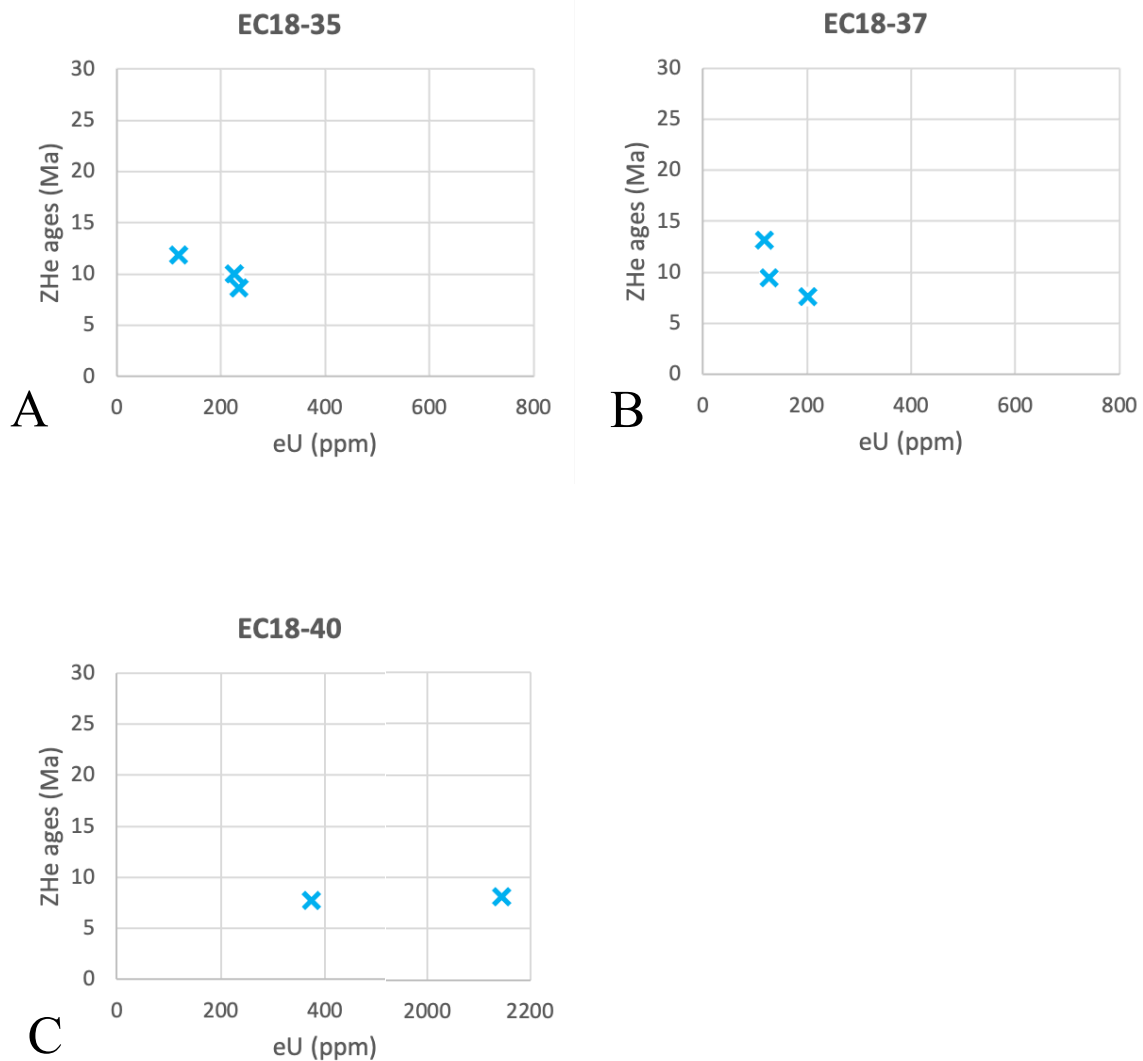


Figure S7: ZHe ages – eU plots for samples from the Apuela area.

Text S3.

Thermal history modeling

Thermal histories were determined using the software QTQt that allows inverting AFT annealing and AHe diffusion parameters using a Bayesian Markov chain Monte Carlo approach (Gallagher *et al.*, 2009; Gallagher, 2012) for complete vertical profiles. The inversion code incorporates kinetic models of He diffusion in apatite (Flowers *et al.*, 2009; Gautheron *et al.*, 2009) and an AFT multi-kinetic annealing model (Ketcham *et al.*, 2007). The modeling procedure is detailed in Gallagher (2012). The input parameters used to

model each profile were the AFT grain count data, the track length distribution, the Dpar values, and the single-grain AHe ages with grains sizes and chemical characteristics. The ZHe thermochronometer is sensitive to temperature ranging from 200 to 20°C depending on the radiation damage of the zircons (Guenther *et al.*, 2013; Ginster *et al.*, 2019; Ault *et al.*, 2019). The ZHe thermochronometer has a wide range of temperature sensitivity depending of the damage of the zircons (e.g., Ault *et al.*, 2019), all the cause for age dispersion are not recognized yet. As our ZHe data did not show a clear correlation between the single grain ages and eU and we were not able to reproduce the measured ZHe ages with the diffusion model included in QTQt (i.e., Guenther *et al.*, 2013), ZHe data were excluded from the modeling.

For the Ibarra profile the beginning of the thermal history model is fixed at $t = 17 \pm 6$ Ma and $T = 800 \pm 50^\circ\text{C}$ based on U-Pb crystallization ages (12.9 ± 0.4 Ma, 23.9 ± 0.7 and 15.4 ± 0.5 Ma; Schütte *et al.*, 2010; this study). For the Guaranda profile, based on U-Pb crystallization ages (25.5 ± 2.4 Ma and 21.0 ± 0.6 Ma; respectively from Schütte *et al.*, 2010 and this study), the beginning of the model is fixed at $t = 23 \pm 3$ Ma and $T = 800 \pm 50^\circ\text{C}$. For the Cuenca profile the beginning of the model is fixed at $t = 16 \pm 3$ Ma and $T = 800 \pm 50^\circ\text{C}$ based on U-Pb crystallization ages (14.8 ± 0.4 Ma and 16.9 ± 0.4 Ma; respectively from Schütte *et al.*, 2010 and this study). For all the areas, at 0 Ma, the temperature was fixed at $5 \pm 5^\circ\text{C}$ for the upper most sample and the atmospheric temperature gradient was fixed at $7^\circ\text{C}/\text{km}$.

Thermal history simulations are the product of 100,000 iterations, that were sufficient to obtain stable and robust solutions (e.g., discussion in Gallagher, 2012). For all models, the grain chemical composition range (and hence potential radiation damage) was taken into consideration following Gautheron *et al.* (2013). We performed simulations using the AFT annealing model of Ketcham *et al.* (2007) and the He radiation-damage model of Gautheron *et al.* (2009) for all three profiles. The results are reported in Fig. 4.

Table S1. Analytical Settings for U-Pb Geochronology at the Arizona LaserChron Center (Element 2 Single Collector).

Table S2. Zircon U-Pb analyses of standards.

Tables S3-S24. Apatite fission-track lengths measurements from all the samples (Western Cordillera, Ecuador).